THESIS

RAPID ACUTE DOSE ASSESSMENT USING MCNP6

Submitted by

Andrew Steven Owens

Department of Environmental and Radiological Health Sciences

In partial fulfillment of the requirements

For the Degree of Master of Science

Colorado State University

Fort Collins, Colorado

Spring 2017

Master's Committee:

Advisor: Alexander Brandl

Thomas Johnson
James Lindsay

ABSTRACT

RAPID ACUTE DOSE ASSESSMENT USING MCNP6

Acute radiation doses due to physical contact with a high-activity radioactive source have proven to be an occupational hazard. Multiple radiation injuries have been reported due to manipulating a radioactive source with bare hands or by placing a radioactive source inside a shirt or pants pocket. An effort to reconstruct the radiation dose must be performed to properly assess and medically manage the potential biological effects from such doses. Using the reference computational phantoms defined by the International Commission on Radiological Protection (ICRP) and the Monte Carlo N-Particle transport code (MCNP6), dose rate coefficients are calculated to assess doses for common acute doses due to beta and photon radiation sources. The research investigates doses due to having a radioactive source in either a breast pocket or pants back pocket. The dose rate coefficients are calculated for discrete energies and can be used to interpolate for any given energy of photon or beta emission. The dose rate coefficients allow for quick calculation of whole-body dose, organ dose, and/or skin dose if the source, activity, and time of exposure are known. Doses are calculated with the dose rate coefficients and compared to results from the International Atomic Energy Agency (IAEA) reports from accidents that occurred in Gilan, Iran and Yanango, Peru. Skin and organ doses calculated with the dose rate coefficients appear to agree, but there is a large discrepancy when comparing whole-body doses assessed using biodosimetry and whole-body doses assessed using the dose rate coefficients.

ACKNOWLEDGEMENTS

I would like to thank my advisor, Dr. Alexander Brandl, for his guidance and support of my research. This project could not have been done without his knowledge and his patience to work with me. My experience with Dr. Brandl will undoubtedly prove invaluable later in my life and my career. His approach to problem solving and ways of thinking helped make this project enjoyable, interesting, and ultimately successful.

I would also like to thank my peers in the program. The comradery we built over my two years at CSU fostered a great experience in Fort Collins, and they kept me sane enough to complete my research. Matt Gift and his ability to help me reason through many questions that came up during my research. J.C. Fisher, Daniel Workman, and Rion Marcinko deserve a ton of credit for letting me run countless simulation hours on their computers. Also, Justin Bell and John Brogan for their constant support and pushing me to get done sooner rather than later.

I would like to thank everyone else who supported me during my research: Dr. Luiz Bertelli for the project idea and his feedback, Kevin Capello for providing me with the MCNP phantom, Steve Sugarman for sitting down and helping me start the project, Dr. Thomas Johnson and Dr. James Lindsay for serving on my committee, and all others who contributed to the work.

Finally, I would like to express my deepest appreciations to my parents, Paula and Steve, and my brother, Jacob. Along with the Collins and Killions, their continued support from Tennessee has kept me going and drives me to be the best I can be. Thank you all for making me the person I am today.

TABLE OF CONTENTS

Introduction

The purpose of this project is to develop a means of rapidly estimating skin, organ, and whole-body doses from high activity external radiation sources after a source has been placed in close proximity of an individual's body (e.g. either in a shirt breast pocket or pants pocket). The motivation for this project is provided by radiation accidents that have occurred in the past due to the misplacement of high activity radiation sources and which have resulted in acute doses to the individuals involved. The individual receiving the dose will be represented by Reference Man or Reference Woman (collectively referred to from hereon as reference persons) as defined by the International Commission on Radiological Protection (ICRP) (ICRP, 2002). The reference persons' whole body, organ, and skin doses are calculated using Monte Carlo methodologies for beta, gamma, and x-ray sources. The simulation results for discrete beta, gamma, and x-ray energies are used to interpolate for doses from radiation energies other than the discrete energies simulated. The dose rate coefficients calculated will be used to retrospectively assess acute dose and validated by comparing doses calculated with the coefficients to published data from past accidents.

Radioactive Decay

The nucleus of an atom is comprised of neutrons and protons, collectively referred to as nucleons. Two fundamental forces in nature significantly influence the nucleus, the strong nuclear force and the electromagnetic force. The strong nuclear force binds the nucleons together, but it only has a range of femtometers. The strong nuclear force is powerful enough to overcome the electromagnetic force which causes like charges, in this case protons, to repel each other. As the number of protons increases, the nucleus becomes larger and requires more neutrons to bind the nucleus together. If the proton-to-neutron ratio is too high or too low to

balance the two forces, the nucleus is unstable and will emit particles to become stable. A nucleus with a particular set of protons and neutrons is called a nuclide. For example, ^{12}C is a nuclide of carbon that contains six protons and six neutrons. (Turner, 2007)

While all nuclei of a given element contain the same number of protons, it is observed that atoms of a single element can have variations in the number of neutrons. For example, magnesium is defined as having twelve protons, but three stable species of magnesium exist having twelve, thirteen, or fourteen neutrons. These different species of the same element are called isotopes, atoms that contain the same number of protons but differ in the number of neutrons. The total number of protons and neutrons an atom has is the atomic mass number. Isotopes of a single element are not equally abundant in nature, with the abundance, for example, of ^{24}Mg, ^{25}Mg, and ^{26}Mg being 79%, 10%, and 11%, respectively (NNDC). Most elements contain several isotopes and because of the different combinations of protons and neutrons for a given element, not all isotopes of an element are stable. (Cember and Johnson, 2009)

A nucleus is said to be radioactive if it decays. Decay is the transformation from an unstable nucleus to a more stable nucleus via the release of particles such as alpha particles, electrons, positrons, and/or photons. When a nucleus decays, the energy available for release is determined by the difference in the mass of the decaying nucleus (the parent) and the mass of the nucleus to which the parent decays (the daughter). The modes of decay can be classified into one of the following three categories: alpha emissions, isobaric transitions, and isomeric transitions. Of these, isobaric and isomeric transitions are most important to this project. (Cember and Johnson, 2009)

Isobaric Transitions

Nuclear transitions in which the atomic mass number of the daughter is the same as the atomic mass number of the parent are referred to as isobaric transitions. While the total number of nucleons remains constant, the number of protons changes by plus or minus one; the number of neutrons changes accordingly to keep the mass number constant. The types of isobaric transitions are beta emission, positron emission, and electron capture. (Cember and Johnson, 2009)

Beta emission results from a nucleus having a neutron-to-proton ratio that is too high. It is the transformation of a neutron into a proton and an electron where the electron is ejected from the nucleus. The emitted electron is called a beta particle. A beta particle is indistinguishable from an atomic electron. When a beta particle is emitted, an antineutrino is emitted in the same process. The antineutrino is a particle without charge and with negligible mass. The transition can be represented by the formula below. (Cember and Johnson, 2008)

$$ {}^{A}_{Z}X \rightarrow {}_{Z+1}{}^{A}Y + \beta^{-} + \bar{\nu} $$

Since each decay releases a specific amount of energy and there are two particles released, the total energy available has to be divided between the beta particle and the antineutrino. Therefore, the beta particle emitted may have an energy from a distribution of possible energies. The energy distribution for the beta particle has a maximum value which occurs when the antineutrino has negligible kinetic energy. When discussing beta emitters, the energy that is released via the decay is reported as either the maximum energy or the average energy of the beta particle energy distribution. As a rule of thumb, the average energy is about one-third the maximum possible energy of the beta. (Cember and Johnson, 2008)

Positron emission results from a nucleus having a neutron-to-proton ratio that is too low. A positron is almost identical to a beta particle except that a positron has a positive charge. The emission of a positron is the result of the transformation of a proton into a neutron and a positron. A neutrino is emitted along with the positron. As with beta emission, the resulting energy that is released from the nucleus is divided between the positron and neutrino, so there is an energy distribution that describes which energies each may have. The rule of thumb applies for positron emission also; the average energy of the positron is about one-third the maximum possible energy. The transition can be represented by the formula below. (Cember and Johnson, 2008)

$$ {}^{A}_{Z}X \rightarrow {}^{A}_{Z-1}Y + \beta^{+} + \nu $$

A third isobaric transition is electron capture (EC) which competes with positron emission. If the neutron-to-proton ratio is too low in a nucleus, then the nucleus may absorb an orbital electron from an inner electron shell and combine it with a proton to create a neutron. The nucleus will usually undergo EC if the unstable parent's mass is less than two electron masses heavier than the daughter. Physically, the energy conservation requirements for EC are easier to satisfy than for positron emission. The transition can be represented by the formula below. (Cember and Johnson, 2008)

$$ {}^{A}_{Z}X + e^{-} \rightarrow {}^{A}_{Z-1}Y + \nu $$

As shown above, only a neutrino is emitted when EC occurs. Since it is the only particle emitted, the neutrino is monoenergetic. After the transition occurs, there is an electron vacancy in the inner shell (typically K-shell) of the electron cloud. It is energetically preferred for electrons to fill inner shells when possible, so an electron from an outer shell (e.g., L-shell) will fill the vacancy. When this occurs, a characteristic x-ray is emitted. The x-ray has an energy

equal to the energy difference between the two electron shells, and is characteristic of the daughter since it occurs after the transformation. Another transition that can occur when there is a vacancy in a lower electron shell is the emission of an Auger electron. This occurs when, for example, an L-shell electron is ejected after a different L-shell electron drops to fill the K-shell, thereby leaving two vacancies in the L-shell. This transition is typical of elements with low atomic numbers. (Turner, 2007)

Isomeric Transitions

Nuclear transitions in which neither the atomic mass number nor the atomic number change from the parent to the daughter are referred to as isomeric transitions. In these transitions, either a gamma or electron is ejected. The two types of isomeric transitions are gamma emission and internal conversion. (Turner, 2007)

One isomeric transition is gamma emission. After either alpha decay or an isobaric transition, the daughter nucleus can be left in an excited state. As electrons emit a characteristic x-ray when they transition from a higher to a lower energy shell, excited nuclei also emit characteristic energies in the form of gamma rays as they transition from higher excited states to lower excited states or the ground state. For example, ^{137}Cs transitions to ^{137}Ba via beta emission. Typically, the ^{137}Ba nucleus is left in an excited state that is approximately 662 keV above its ground state. Thus, the nucleus will de-excite by releasing a 662 keV gamma ray. Although the gamma ray is emitted by the daughter ^{137}Ba, the 662 keV gamma ray is called the "^{137}Cs gamma ray." One reason for this is that typically the "lifetime" of the excited nuclear state is about 10^{-10} seconds, although there are exceptions, as in the example provided. The mean life of the excited state of ^{137}Ba is about 3.6 minutes. When the excited state exists for a long time relative to 10^{-10} seconds, the excited state is called metastable and is denoted as ^{137m}Ba. (Turner, 2007)

Internal conversion occurs when the energy of an excited nuclear state is transferred to an atomic electron which is then ejected from the atom. The electron has an energy equal to the energy of the atomic transition minus the binding energy of the electron that was knocked out of its shell. As with EC, when an electron from an inner shell is ejected, an outer shell electron will fill the vacancy producing characteristic x-rays or Auger electrons. Internal conversion is typically more prevalent in heavier nuclei, while gamma emission is more typical in lighter nuclei. (Turner, 2007)

Activity

The activity of a radioactive source is defined as the number of decays within a given time interval. Activity can be measured in Becquerels (Bq) or Curies (Ci). A Becquerel is the number of nuclear transformations per second, and a Curie is defined as the amount of activity that one gram of ^{226}Ra exhibits. The conversion between the two units is 1 Ci is equal to 3.7 x 10^{10} Bq. It should be noted that 1 Bq does not imply that one particle is emitted per second, because a single nuclear transformation can emit multiple particles. (Cember and Johnson, 2008)

The activity of a radioactive source decreases exponentially over time. The rate at which this decrease occurs can be described by the half-life ($H_{1/2}$), the time it takes for half of the atoms to undergo a transformation. Half-lives can range from fractions of a second to many years. The activity of the source can be found after some time (t) if the original activity (A_0) is known using the following equation:

$$A = A_0 e^{-\frac{\ln(2)t}{H_{1/2}}} \quad (1)$$

Electron and Positron Interactions with Matter

Electrons and positrons interact with matter in very similar ways, because they are identical particles except for having opposite charge. The particles lose energy due to

electromagnetic interactions and collisions. The electromagnetic force acting on the charged particles can result in a change of velocity and/or direction. When an electron or positron's velocity or direction is changed, it releases photons. The photons released are referred to as Bremsstrahlung radiation.

Collisional interactions for electrons and positrons are generally with atomic electrons of the medium with which they are travelling through. Both particles can have large scattering angles with their targets, and they can lose a large fraction of their energy in single collisions. If a positron collides with an electron, they will annihilate and become two photons with at least 511 keV that travel in opposite directions. (Cember and Johnson, 2008)

Photon Interactions with Matter

Photons encompass both gamma rays (photons emitted from the nucleus) and x-rays (photons emitted from atomic orbitals). They can travel a longer distance than most radiation before interacting with the medium through which they are travelling. The interactions are governed by statistical probabilities of interaction. The probability of interaction is dependent on both the material the photons are passing through and the energy of the photons. The main mechanisms of interaction are photoelectric effect, Compton scattering, and pair production. (Turner, 2007)

The photoelectric effect is the dominant interaction for low energy photons, those that have energy less than approximately 100 keV. During the photoelectric effect, a photon deposits its energy to a bound electron causing the electron to be ejected from the atom. For this to occur, the incoming photon must have an energy greater than the binding energy of the electron. Therefore, the electron leaves the atom with an energy equal to the energy of the photon minus the binding energy of the electron. The probability of this effect occurring decreases rapidly as

energy increases, but the probability increases if the medium is a high-Z material (where Z is the atomic number). The probability roughly varies as Z^4/E^3, where E is the energy of the photon. (Turner, 2007)

Compton scattering is the dominant interaction for intermediate energy photons, photons with an energy between 0.1 MeV and 10 MeV. Compton scattering is the phenomenon of a photon scattering with a free electron, an electron in an outer atomic shell that is only loosely bound to the atom. The photon can lose negligible energy or a large fraction of its energy depending on the angle through which it scatters. A photon that scatters back in the direction that it came from loses the most energy versus a photon that has a low scattering angle and is only slightly deflected that loses almost no energy. The probability of Compton scattering occurring increases as the atomic density and atomic number increase. (Tuner, 2007)

A third main mechanism of interaction for photons is pair production. It is the most prominent effect for highly energetic photons with energies on the order of or above 10 MeV. Pair production may occur when a photon is near an atomic nucleus and has an energy of greater than 1.022 MeV. The photon transforms into an electron and a positron, with the kinetic energy of the two particles equaling that of the initial photon minus 1.022 MeV, the mass energy of the two particles. The electrons and positrons then interact as discussed previously, with the positron producing annihilation photons. The probability of pair production increases with energy and atomic number approximately as Z^2. (Turner, 2007).

Photon interaction is governed by statistical probabilities. The probability of interaction per unit path length is represented by μ and is called the attenuation coefficient. The attenuation coefficient has units of inverse length (e.g. cm^{-1}). Monoenergetic photons are attenuated

exponentially. If the monoenergetic photons are traveling in a beam, they are attenuated based on the equation:

$$N = N_0 e^{-\mu t} \quad (2)$$

where *N* is the number of photons that have not interacted, N_0 is the original number of photons and *t* is the distance traveled in the medium. (Turner, 2007)

Measurable Quantities

Radiation damage is dependent on how much energy is absorbed from radiation interacting in a medium. The unit of absorbed dose is the Gray (Gy) which is defined as one Joule of radiation energy absorbed in a mass of one kilogram. A unit that is sometimes used instead of the Gray is the rad (radiation absorbed dose). A rad is 100 ergs absorbed in a mass of one gram, and is equal to 0.01 Gy. Absorbed dose is referred to as a "physical quantity" because it can be measured directly. There are other measurable quantities that can be related to dose that are used in the field of health physics which include fluence and kerma. (Cember and Johnson, 2008)

Fluence is defined by the ICRP as "the quotient of d*N* by d*a*, where d*N* is the number of particles incident on a sphere of cross-sectional area d*a*" (ICRP, 2007). Fluence can be related to dose if other factors are known such as the energy distribution of the particles, the fraction of the energy absorbed by the target, and the mass of the target. For example, a common method of calculating skin dose is using conversion coefficients published by the ICRP that convert particle fluence in units of particles per cm^2 to absorbed dose in pGy. There are also conversion coefficients for other organs in the body. (ICRP, 1996)

Kerma is the kinetic energy released by a particle into the material through which it is traversing. Kerma may be used to approximate the absorbed dose if electronic equilibrium has

been established. Electronic equilibrium exists in a volume if the amount of energy carried out by secondary particles is also deposited by incoming secondary particles. Electronic equilibrium cannot be assumed if material near the volume of interest is made up of vastly different material or if the radiation field varies considerably across the volume in question (Shultis and Faw, 2000). For tissue, kerma approximates absorbed dose well for photons up to 300 keV at which point kerma starts to overestimate absorbed dose (Veinot and Hertel, 2007).

Protection Quantities

Special quantities called "protection quantities" were defined by the ICRP "in order to relate the radiation dose to radiation risk (detriment)… [and] take into account variations in the biological effectiveness of radiations of different quality as well as the varying sensitivity of organs and tissues to ionising radiation" (ICRP, 2007). The protection quantities currently used by the ICRP were introduced in 1990 (ICRP, 1991). The protection quantities are equivalent dose and effective dose, and they are directly comparable to maximum recommended doses to individuals as determined by the ICRP.

Equivalent dose considers how damaging different types of radiation are as they interact with the body. Equivalent dose is the absorbed dose in a tissue or organ multiplied by the radiation weighting factor. The radiation weighting factor is higher for more damaging radiation. The value of the radiation weighting factor for both photons and beta particles is 1. The unit of equivalent dose is the Sievert (Sv) which is equal to one Joule per kilogram. The special unit Sievert is used to signify that the reported dose has been multiplied by a weighting factor as opposed to absorbed dose which is measured in Gray, and the Sievert can be directly related to detriment. (ICRP, 1991)

Effective dose (E) considers how sensitive different organs and tissues are to radiation. Effective dose is defined as "the sum of the weighted equivalent doses in all tissues and organs of the body, given by the expression $E=\Sigma_T w_T H_T$, where H_T is the equivalent dose in organ or tissue T, and w_T is the weighting factor for tissue T" (ICRP, 2007). The tissue weighting factors are given in Table 1. The unit for effective dose is also the Sievert. Not every individual's tissues and organs respond the exact same way to radiation, so it is important to note the tissue weighting factors recommended by the ICRP are sex-averaged and age-averaged. The implication of averaging is that the tissue weighting factors are "restricted to the determination of effective dose in radiological protection and, in particular, cannot be used for the assessment of individual risk" (ICRP, 2007).

Table 1: ICRP Tissue Weighting Factors (ICRP, 2007)

Tissue	w_T	$\sum w_T$
Red bone-marrow, Colon, Lung, Stomach, Breast, Remaining Tissue	0.12	0.72
Gonads	0.08	0.08
Bladder, Oesophagus, Liver, Thyroid	0.04	0.16
Bone surface, Brain, Salivary glands, Skin	0.01	0.04

External Dose

External dose is applied to a body when the radioactive source is located external to the body. Typically, external sources are not of concern because many precautions can be taken to minimize the dose. External dose can be of major concern, however, if a highly active source is orphaned or mishandled. Three principles that can be considered to minimize the dose are time, distance, and shielding. The dose decreases when the following occur: time spent with the source

decreases, distance from the source increases, and shielding around the source increases. (Sugarman and Toohey, 2013)

The health concern for an external source is usually damage to the skin because that is the first organ with which the radiation will interact. The most damaging type of radiation to the skin is beta particles. Distance is crucial when trying to reduce the absorbed dose because radiation intensity tends to follow the inverse-square law, meaning that as distance increases by a factor of two the fluence, or intensity, decreases by a factor of four. (Sugarman and Toohey, 2013).

Reference Persons and Computational Phantoms

Reference persons are used in the health physics community to best estimate the effects of radiation exposure to the human population. The current reference persons are defined by reference values published by the ICRP (ICRP, 2002). The reference values compiled by the ICRP are based on data for Western Europeans and North Americans because they were the most studied and understood populations at the time of publication. Therefore, the values best represent that population, and it is understood that the average person for other populations may vary greatly from the reference values. For example, "the mass of fat in an adult male from China is only around 50% the reference value" (ICRP, 2002). Also, the reference values, like the tissue weighting factors, represent average values of a population, with respect to both age and gender, so any retrospective dosimetry following an exposure should use known data from the exposed individual in favor of the reference values.

Computational phantoms are computer models of the human anatomy that are used in the field of health physics to calculate doses to humans. Before computational phantoms, physical phantoms made of tissue and/or bone equivalent material were used to simulate exposures by placing detectors inside the phantom and exposing them to radiation. Computational phantoms

became increasingly popular after computer codes were developed to simulate radiation transport during nuclear testing research in the 1940s. Since the development of computational phantoms (henceforth referred to as phantoms) over 120 phantoms have been reported in various literature concerning ionizing and nonionizing radiation. Over the years, the sophistication of phantoms has evolved greatly, and there are currently three different types of phantoms: stylized, voxelized, and boundary representation (BREP). (Xu and Eckerman, 2010)

Stylized phantoms were the first iteration of phantoms that were initially developed by Fisher and Snyder at Oak Ridge National Laboratory (ORNL) during the 1960s (Fisher and Snyder, 1966). A stylized phantom utilizes simple three dimensional geometries that can be modeled by quadratic equations to represent anatomical features (e.g. cylinders for arms, half ellipsoids for lungs). Stylized phantoms are easily modeled; however, because the human anatomy is extremely complex, they do not provide the best representation of the human body. Due to the advancement of computer capabilities and the development of anatomically more accurate phantoms, stylized phantoms became outdated in the 1990s. (Xu and Eckermen, 2010)

Voxelized phantoms were the next evolution of phantoms, and started being developed during the 1980s. Voxelized phantoms model human anatomy by utilizing three-dimensional images from Computer Tomography (CT) scans or Magnetic Resonance Imaging (MRI). A voxel is a three-dimensional pixel, and can be thought of as a building block. A user or a program must specify which regions of the digital image represent the different organs/tissues, assign properties such as density and chemical properties, and convert the new segmented image to a file that can be read by a radiation transport code. The biggest advantage of the voxelized phantom over the stylized phantom was that a voxelized phantom could be created to represent a specific person. A problem with voxelized phantoms is that they do not have smooth surfaces

since they are made up of three-dimensional cubes. Voxelized phantoms are also difficult to alter, so the phantom is only useful for the particular individual used to create the model. (Xu and Eckerman, 2010)

The voxelized phantoms were the most evolved form of the computational phantom until the 2000s when the first BREP phantoms were developed. BREP phantoms also utilize three dimensional imaging to create the phantoms, but instead of using voxels, they are created out of polygonal meshes. Polygonal meshes are smooth and can be more easily altered (e.g. stretched or compressed) to model different individuals. Some BREP phantoms are dynamic such as the 4D Cardiac Torso (NCAT) phantom which models cardiac and respiratory motions. BREP phantoms are currently the most advanced phantoms available for radiation transport simulation. (Xu and Eckerman, 2010)

Deterministic Effects and Acute Radiation Syndrome

Deterministic effects of radiation have a dose threshold associated with them, below which the effect generally is not observed in an exposed individual. Deterministic effects become more severe as the dose increases. Some examples of deterministic effects are nausea/vomiting (~1 Gy), skin erythema (~3 Gy), headache (~4 Gy), and loss of consciousness (~8 Gy) (IAEA, 1998). Deterministic effects are mostly of concern when there is a large dose delivered over a short period of time (a few hours or shorter). When this occurs, the delivered dose is called an acute dose and can result in acute radiation sickness.

Acute radiation sickness or acute radiation syndrome (ARS) is a potentially lethal effect that occurs from a whole-body exposure of roughly 1 Gy or higher (Hu, 2016). ARS typically will manifest itself within the first 30 days of exposure, and the symptoms include vomiting, diarrhea, headache, fever, and loss of consciousness. One form of classification of ARS is

described by the International Atomic Energy Agency (IAEA) in five categories: mild (1-2 Gy), moderate (2-4 Gy), severe (4-6 Gy), very severe (6-8 Gy), and lethal (>8 Gy) (IAEA, 1998). While the IAEA has defined the lethal dose as one over 8 Gy, it is accepted that a dose of about 4 Gy will result in about 50% deaths in a population within 30 days; this dose is referred to as the LD_{50} (lethal dose to 50% of the population) (Turner, 2007).

Industrial Radiography Sources

A common source of acute radiation exposures are radiography sources. Radiography utilizes photon interactions to obtain a picture of an object. One example of this is an x-ray machine. An x-ray machine can be used to determine if a bone is broken by sending x-rays through the patient. Most of the x-rays will interact with the bone; however, if there is a break or fracture, some x-rays will pass through the break with little interactions occurring and create a contrast on the film.

Industrial radiography utilizes the principles of radiography to detect defects in manufactured parts or building structures. Industrial radiography is used to examine gas and oil pipelines, pipes, and pressure vessels in chemical plants, vehicles, and aircraft (National Research Council, 2008). Most of the structures that are examined are made of concrete, steel, and/or other metals. In order to penetrate these materials, higher energy gamma rays have to be used as opposed to typical medical x-rays which generally have a range of 100 eV – 100 keV. Some sources that are commonly used for industrial radiography are: ^{60}Co (average gamma energy of 1,250 keV), ^{192}Ir (380 keV), ^{75}Se (217 keV), and ^{169}Yb (145 keV) (National Research Council, 2008).

Although using radionuclide radiography is convenient due to the small size and mobility of the device, there are safety hazards associated with the sources. The radiography source is

normally inside a housing that shields workers from the exposure when it is not in use. However, when the source is being used, it creates radiation fields that can be extremely dangerous. In 2005, personnel working in gamma radiography had an average total effective dose of 5.2 mSv compared to 1 mSv for workers in commercial nuclear power reactors (National Research Council, 2008). Due to the energies and high activities (on the order of GBq or TBq) of the sources, the sources can cause overexposures and acute radiation injuries if mishandled.

Accidents

The IAEA generates and publishes reports on radiological accidents that occur around the world. These reports give details of the accidents and the responses to each accident. The reports cover a wide range of types of events such as the Fukushima power plant incident, overexposures to radiotherapy patients, overexposures from bypassing safety features at facilities, and overexposures from picking up an orphaned source. Of the nineteen accidents covered in the past, two will be focused on in this study: the radiological accident in Gilan, Iran and the radiological accident in Yanango, Peru. These accidents were selected because they both involve a person picking up misplaced radiography sources and placing the source in a pocket.

The accident in Gilan, Iran occurred on July 24, 1996 at a fossil fuel power plant. The radiography source involved was a 185 GBq ^{192}Ir source that accidentally dropped off its cable and fell into a trench after it was used by a radiography team to check a pipe. The radiography team assumed the source was safely in its housing because they could not detect the source with their instrumentation. However, they could not detect the source because it was shielded by concrete when it was down in the trench. At approximately 08:00, a worker at the plant discovered the source, and placed it in the right breast pocket of his overalls where it remained for the next 1.5 hours (periodically being momentarily removed as the worker observed it). After

the 1.5 hours, the worker returned the source to the trench as he began experiencing dizziness, nausea, and a burning feeling on his chest. Meanwhile, the radiography team noticed the source was missing and recovered it about 30 minutes after the worker returned it to the trench (approximately 10:00). It was unknown to the radiography team that the source had ever been handled by another person. The exposed worker was sent the hospital several hours later (13:00). It is estimated that the worker received a whole-body dose of about 3-4 Gy and a localized dose of about 40 Gy to his palm from handling the source. (IAEA, 2002)

The accident in Yanango, Peru occurred on February 20, 1999 at the Yanango hydroelectric power plant. The source involved was a 1.37 TBq ^{192}Ir source that was being used to investigate the repair of a pipe. The radiography team arrived at 11:30 to verify a pipe had been welded correctly; however, when the team arrived, the weld was not complete, and the welding crew was out to lunch. The radiography team left the source housing (with the source in it) and the rest of the equipment at the sight unsupervised while they went to lunch. At some unknown point during the day, the ^{192}Ir source became detached from the housing, and a welder picked it up with his right hand and put it in his back pants pocket at approximately 16:00. The welder worked until 22:00 when he took a bus home. He removed his jeans at approximately 22:30 after complaints to his wife of a pain on the back of his upper thigh. The source in the meantime was discovered missing by the radiographers, and tracked to the welder's house at about 1:00 on February 21. During the time the welder had the source he was exposed, but also exposed everyone on the bus that he took home, his wife, and his 18 month old child. The welder's whole body dose was estimated to be about 1.2 Gy, but dose to his femur was estimated between 5 and 15 Gy. The skin dose on the surface of the skin at a point 3 cm from the center of

the skin lesion that formed was estimated to be 100 Gy. The radiation injury to his leg resulted in his leg having to be amputated. (IAEA, 2000)

Materials and Methods

The Monte Carlo N-Particle 6 (MCNP6) (Los Alamos National Lab) transport code was used to simulate the radiation transport. MCNP6 allows the user to specify three-dimensional geometries using simple surfaces such as planes, spheres, and cylinders in a Cartesian coordinate system with each surface having a unique surface number. The surfaces are used to define cells which have unique cell numbers. All space must be defined for the MCNP model, and no cells can overlap with one another.

The ICRP computational reference phantoms for the adult male and the adult female phantom were used as the geometries for the simulations. Both are voxelized phantoms which were provided in their MCNP6 input form by Kevin Capello at Health Canada. Each phantom is made up of a lattice of voxels. The geometries were checked to ensure they matched the parameters given by the ICRP. The male adult reference phantom is 1.76 meters tall (~ 5' 9") with a mass of 73.0 kg (weight of about 161 pounds). He is made up of 1,946,375 voxels, each with a volume of 36.54 mm^3. The female adult reference phantom is 1.63 meters tall (~ 5' 4") with a mass of 60.0 kg (weight of about 132 pounds). She is made up of 3,886,020 voxels, each with a volume of 15.25 mm^3. There are 139 organs identified for each phantom with each of them having a unique organ identification number. The identification numbers and associated organs are listed in Appendix A. These organ numbers were also used as cell numbers for the voxelized phantom, with each organ being represented by a cell. (ICRP, 2009)

MCNP6 requires the user to define a radiation source in the geometry. For each of the phantoms, an unshielded breast-pocket source and unshielded back-pocket source were defined in space by using a visualization tool, Visual Editor (VisEd), supplied by the developers of MCNP6. VisEd allows the user to look at the geometry in two-dimensional cross sections as

shown in Figure 1. Each of the voxelized phantoms is defined in a rectangular prism with minimum coordinate (0, 0, 0) and maximum coordinate (54.2798, 27.1399, 177.6) and (53.0725, 24.3175, 168.432) for the male and female, respectively. The position coordinates for the breast-pocket and back-pocket sources were approximated based on the position of organs shown in the VisEd view and are listed in Table 2. Sources must also be assigned an energy distribution and a particle type. All sources were assigned a combination of one distinct energy and one particle type (either photon or beta).

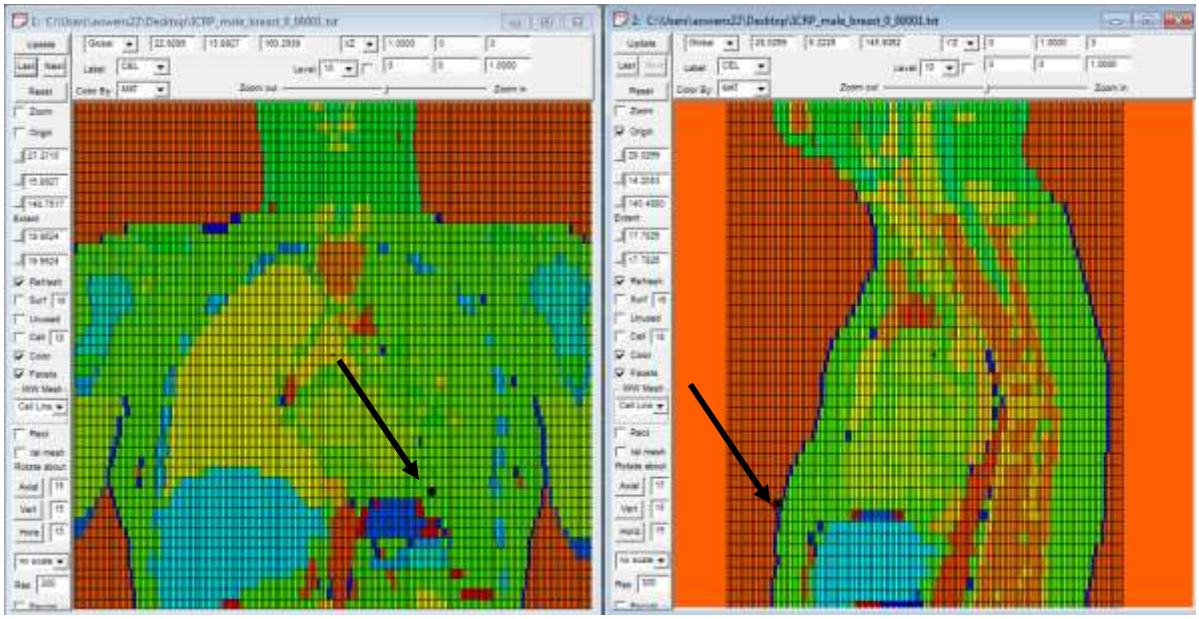

Figure 1: View of voxelized male phantom in VisEd with breast pocket source. Source is represented as black dot with an arrow pointing to it.

Table 2: Important coordinates in the geometries

Description	Gender	Coordinate
Breast-pocket source	Male	(35, 3.4, 130)
	Female	(34.7, 3.5, 130.9)
Back-pocket source	Male	(17, 24.9, 82)
	Female	(16.6, 23.3, 81.5)

Simulations were performed with the reference male and a photon beam with an energy of 50 keV directed at the phantom to verify the simulation, including the physical model and material compositions, was behaving as expected. The beam was positioned at (26 cm, -15 cm, 145 cm) and was directed in the positive y-direction. Photon fluence was tallied by MCNP6 at different points proximal and distal to the phantom and compared to the photon attenuation expected from analytical calculations. The photon fluence was tallied across planes perpendicular to the y-axis at y-positions of (-6 cm, 24 cm, 30 cm).

Simulations were also performed to check if the following assumptions were correct: clothing does not significantly affect organ doses, shielding encapsulating the source does not significantly affect organ doses, and the kerma approximation for absorbed dose is appropriate for organ doses. These simulations used the male phantom with the breast pocket point source of photons with energies of 0.01, 0.1, 1.0, and 10.0 MeV, and compared energy deposited in the organs resulting from simulations performed under those assumptions, one at a time, and for representative parameter sets with those assumptions relaxed. The skin voxels were changed to cloth material to check the clothing assumption. The source was encapsulated by a 1.2 mm tall stainless steel cylinder with a radius of 3.0 mm and thickness of 1.0 mm to check the shielding assumption. The steel is stainless steel 304 as defined by the Pacific Northwest National Lab's *Compendium of Material Composition for Radiation Transport* (McConn Jr et al., 2011). The kerma assumption was checked by running one simulation in photon only mode, meaning that when a photon deposited its energy, all the energy was absorbed at the point of interaction instead of creating secondary particles (this represents the kerma approximation), and another simulation was performed in photon and electron mode, meaning the photon could deposit energy and create secondary electrons with each interaction. These initial tests allowed for the

whole body phantoms to be simulated with no clothing, no shielding encapsulating the source, and using the kerma approximation. The study included a total of 29 different energies simulated for two different particle types (beta and gamma). With the different combinations of gender, source position, energy, and particle type, a total of 232 simulations were performed using MCNP6 and the computational phantoms. The result of the phantom simulations was the energy deposited in each organ in MeV, or an *F8 tally in MCNP6.

Another geometry was created to calculate skin dose. A square slab 15.24 cm wide/tall and 0.15 cm thick was used to approximate the skin, and was made of the same composition used for the skin in the reference computational phantoms. Nineteen centimeters of water were arbitrarily inserted behind the skin to approximate the depth of the body, providing ample material in the geometry for backscattering of particles. The source used to calculate skin dose had a cylindrical stainless steel shield encapsulating it that was 1.0 mm thick, 1.2 mm tall, and had an outer radius of 3.0 mm. The source is placed 5 mm from the edge of the skin. A total of 29 different energies were simulated for the two different particle types, again resulting in 58 total simulations. The results of these simulations were obtained in terms of the fluence of photons or electrons entering the skin over a 10 cm^2 area as defined for shallow dose by the Nuclear Regulatory Commission (NRC) (10 C.F.R. § 10, 2017). The fluence was converted to dose using the conversion coefficients published by the ICRP (ICRP, 1996).

MATLAB (Mathworks, 2016), a computational/data analysis software, was used to transfer the tallies from MCNP6 output files into an Excel file. Different MATLAB scripts were written to calculate organ doses, whole body dose, and skin dose.

Results and Discussion

Benchmarking

The "physics check" simulations are compared to theoretical calculations applying attenuation coefficients. The calculation assumes that the photons were traveling through one of three materials at any point: air, tissue, or bone. A diagram of the geometry through which the beam travels is shown in Figure 2. The attenuation coefficients used in the calculations are shown in Table 3. The distance traveled through each material are approximate and are estimated by looking at the geometry in the VisEd software. The simulation and expected results are shown in Table 4. The fluence is calculated using Equation 2 and represents the fluence of photons that have not interacted. The ratio of fluence not attenuated to original fluence (I/I_0) for the simulations and analytical calculations agree well (within 10%). The uncollided fluence from the MCNP6 results were used as that fluence represents the photons that have not interacted. The

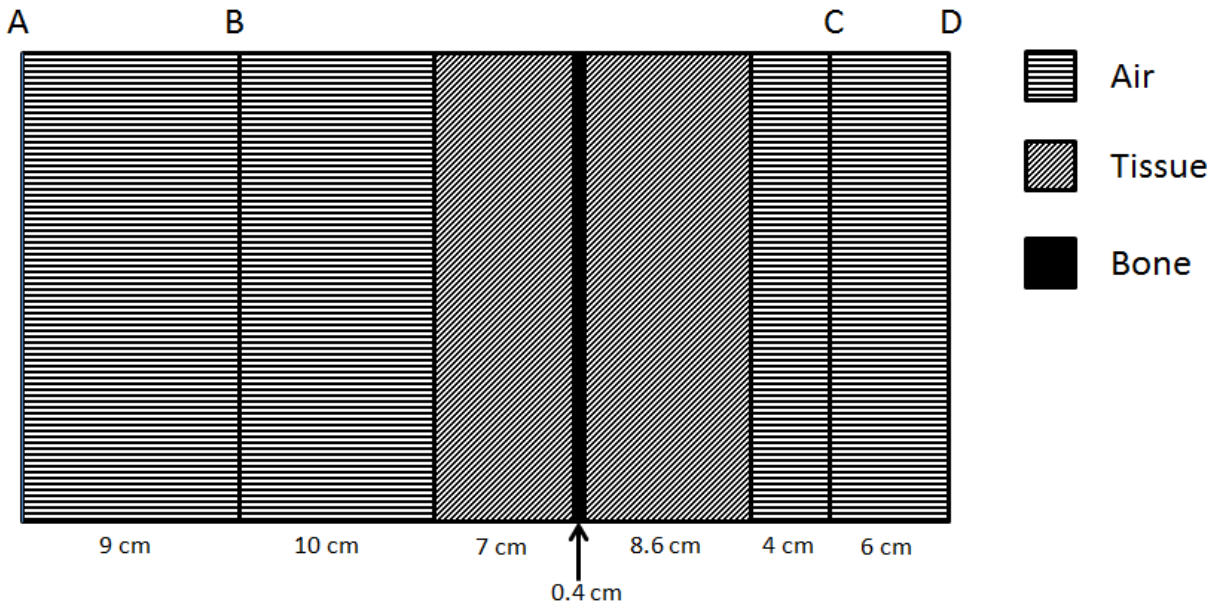

Figure 2: Diagram of the geometry for photon beam attenuation. Planes A, B, C, and D represent where fluence was tallied with MCNP6.

Table 3: Attenuation coefficients

Material	Mass attenuation coefficient ($cm^2\ g^{-1}$)*	Density ($g\ cm^{-3}$)	Attenuation coefficient (cm^{-1})
Air	2.080×10^{-1}	0.001	2.080×10^{-4}
Tissue	2.223×10^{-1}	1.05	0.233
Bone	4.242×10^{-1}	1.90	0.806
*(Johnson and Birky, 2012)			

Table 4: Simulated and calculated fluence attenuation.

Plane	Simulation Result (cm^{-2})	Simulation I/I_0	Calculated I/I_0
A	0.9991	1.0000	1.0000
B	0.9974	0.9983	0.9981
C	0.0180	0.0180	0.0190
D	0.0178	0.0178	0.0190

results indicate that the physics of the computational phantoms provided by Kevin Capello behave as expected and no additional changes to the phantoms is required.

Figure 3 shows the results of comparing the male phantom with a clothed male phantom. The results are shown as percent difference in energy deposited for each cell of the phantom. The percent difference is relative to the original male phantom and a negative percent difference indicates that the clothed phantom has less energy deposited in the particular cell than the male phantom. There are no percent differences outside of ±10% for the simulated energies, indicating that simulating the phantom with no clothes was a fair approximation of the actual dose. It should be noted that the cell/organ with the highest percent difference for each energy is the skin of the trunk with up to a 7% difference. However, it was the skin of the trunk that was changed to clothing for the simulation, so it is about 50% more dense and made of a material that attenuates photons more which results in more energy deposited.

The comparison for the shielded and unshielded source for the male phantom are presented in a similar manner as above in Figure 4. As the energy of the source increases, the

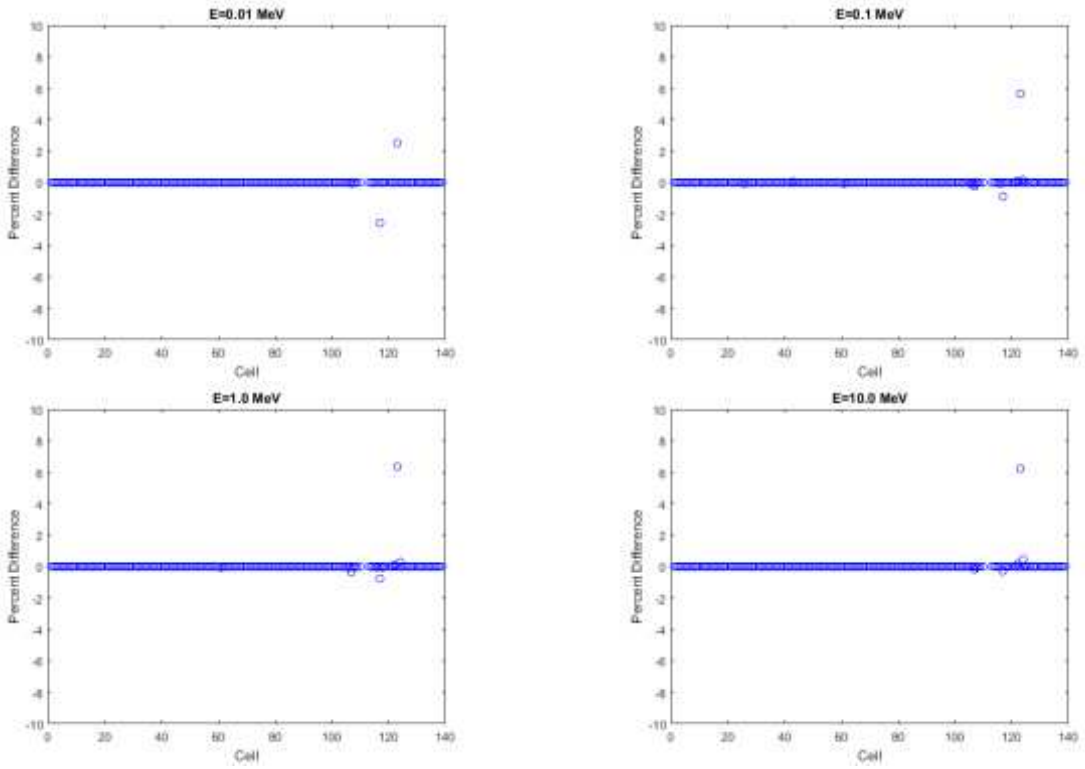

Figure 3: Percent differences in each cell for a clothed and unclothed male phantom.

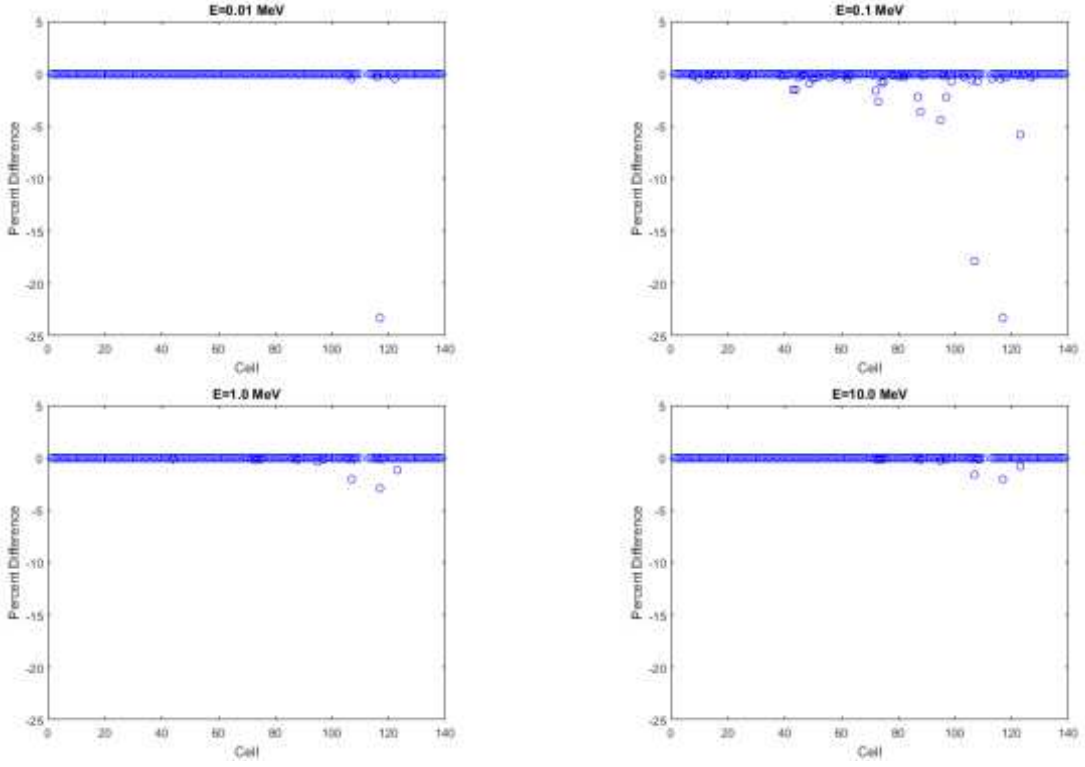

Figure 4: Percent differences in each cell for a shielded and unshielded source for the male phantom.

percent difference between the two simulations appears to decrease meaning that for higher energies the shield becomes less influential on the total dose. The percent differences for 0.01 MeV are not as large as the trend would predict, but this is because for that energy almost all cells get zero or negligible energy deposited even without the shield. The cells that exhibit greater than 10% difference are muscle in the trunk (-17.8% for 0.1 MeV) and residual tissue in the trunk (-23.32% for 0.01 MeV and -23.26% for 0.1 MeV). Based on the results, the whole-body doses can be calculated with the source not encapsulated

Figure 5 shows the comparison for the kerma approximation for the male phantom for different energies. There is no difference for 0.01 or 0.1 MeV which is expected as kerma approximates dose well up to 0.3 MeV (Veinot and Hertel, 2007). At 1 MeV some differences can be seen, but they are all within 5%. There are some differences larger than 10% when the energy of the photons is 10 MeV with the residual tissue of the trunk having a difference of -

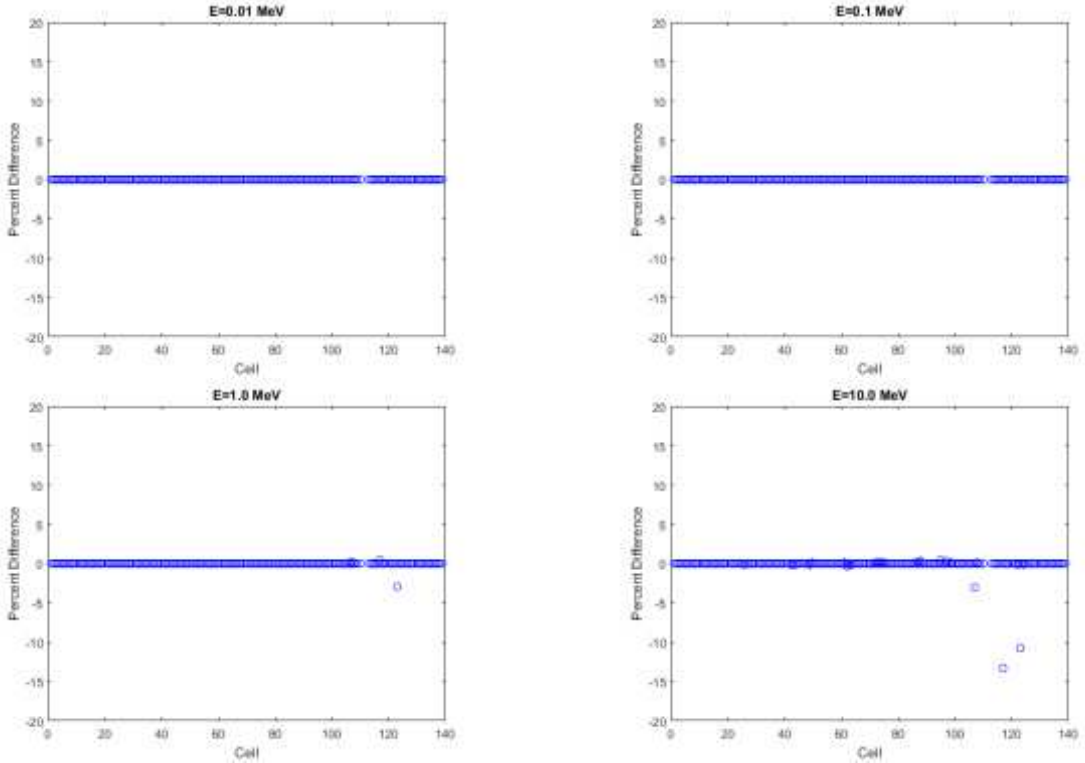

Figure 5: Percent differences in each cell for the kerma approximation for the male phantom.

13.34% and the skin of the trunk having a difference of -10.73%. Besides the skin and residual tissue of the trunk, all other cells have less than 5% deviation for the simulated energies. The kerma approximation can be used for the whole-body dose simulations, based on the results, which agrees with the similar work done by Bellamy et. al. (Bellamy et. al., 2016).

The three approximations discussed above were only checked for the male phantom and photon simulations. It is extrapolated that the male and female phantom would not have significantly different results. Beta particles were not benchmarked separately because it is expected that the absence of clothes, the absence of shielding, and the kerma approximation would all result in an overestimation of the absorbed dose, providing a protective worst case dose estimate.

Breast Pocket Source

The whole-body dose rate coefficients for the male and female phantoms for photon and beta breast pocket sources are plotted in Figure 6 (see Appendix B for tabulated data). The dose rate coefficient, D_C, is calculated using the following equation:

$$D_C = \frac{E_D(1.602\times10^{-13}\ \text{J MeV}^{-1})}{m} \tag{3}$$

where E_D is the energy deposited in the body in units of MeV and m is the mass of the phantom in units of kg (73 kg for the male phantom and 60 kg for the female phantom). The photon dose rate coefficient increases as the energy of the source increases as expected, however the percentage of the source energy deposited initially decreases, but stays between 15 – 20% for males and 10 – 15% for females above energies of 70 keV. The male-to-female whole-body dose rate coefficient ratio is approximately 1 for all photon energies. This means that for a

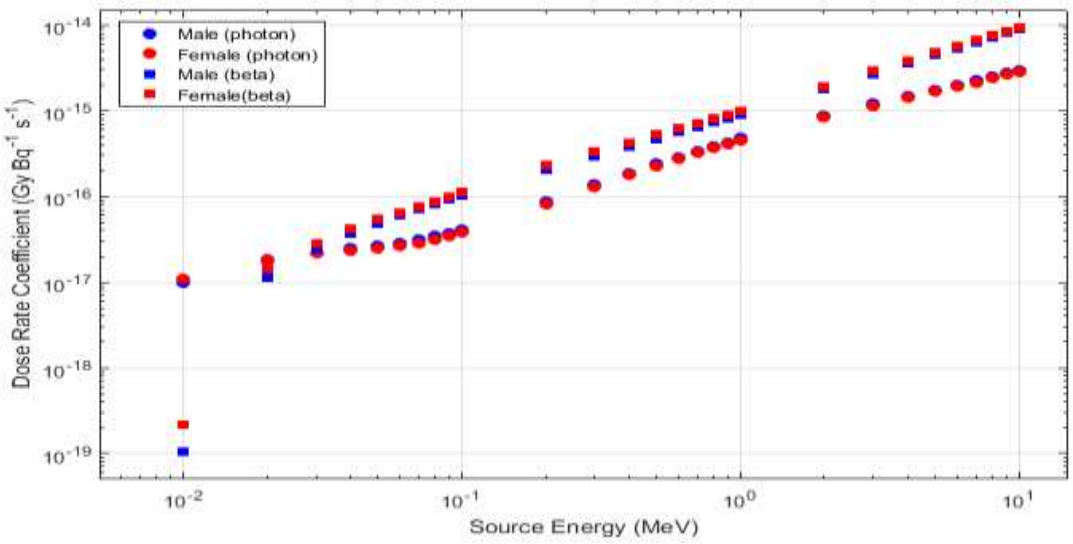

Figure 6: Plot of the whole-body dose rate coefficients for the male and female phantoms for a photon and beta breast pocket sources.

monoenergetic photon source exposure of a given activity and time, the whole-body dose to either the male or female phantom is approximately the same.

The dose rate coefficients for the beta breast pocket source exhibit similar characteristics to those for the photon breast pocket source. However, the ratio between the male and female beta coefficients are not as close to 1.0 but instead range from 0.78 to 0.97 for energies greater than 10 keV. When comparing the dose rate coefficients for gammas and betas at a given energy, the coefficient for beta particles appears to be approximately 2.5 – 3.0 times larger at energies above about 40 keV. However, the photons and gammas have approximately the same dose rate coefficient at about 20-30 keV. Another difference between the photon and beta source is that the beta source deposits about 35 – 45% of its energy for the male phantom and about 35 – 40% for the female phantom. The source was simulated as an isotropic source, so at most 50% of the radiation would go towards the body. Betas are expected to deposit almost all of their energy, so approximately 50% energy deposition is expected for this geometry.

Although the whole-body dose rate coefficient is approximately the same for the male and female phantom, the doses to individual organs vary much more. Table 6 shows dose rate coefficients and male-to-female ratios for the breast and trunk muscle. The dose rate coefficient for each organ is calculated using Equation 3 with the masses given for the organs of the adult phantoms by ICRP (ICRP, 2009). The data used to calculate the organ dose rate coefficients can be found in Appendix C. The male's breast dose rate coefficients for photons of various energies is approximately 0.77 times the coefficient for the female, whereas the coefficient for the muscle in the trunk is approximately 1.2 times that of the female for the male. These organ dose coefficients are shown only to illustrate how different the individual doses to the organs can be, even when the whole-body dose delivered is approximately equal.

The breast tissue and trunk muscle cells are also examined for the beta source, and the results are shown in Table 7. The comparison with the beta source exhibits how greatly the organ dose rate coefficients can differ between the male and female phantoms. The male-to-female organ dose rate coefficient ratio ranges from 0.00478 to 0.780 and 0.0231 to 29.8 for breast tissue and trunk muscle, respectively. This shows there can be differences in orders of magnitude for the organ dose rate coefficients between the two phantoms compared to the ratio range of 0.78 to 0.97 for the whole-body dose rate coefficient ratio between the two phantoms.

Table 6: Photon dose rate coefficient comparison for individual tissues (Dose rate coefficients given in units of Gy Bq^{-1} s^{-1})

	Breast			**Trunk Muscle**		
Energy (MeV)	**M. Coeff.**	**F. Coeff.**	**M/F**	**M. Coeff.**	**F. Coeff.**	**M/F**
0.1	9.28×10^{-16}	1.19×10^{-15}	0.776	4.39×10^{-17}	3.32×10^{-17}	1.32
0.5	5.77×10^{-15}	7.55×10^{-15}	0.765	2.64×10^{-16}	2.10×10^{-16}	1.26
1	1.10×10^{-14}	1.43×10^{-14}	0.765	5.34×10^{-16}	4.37×10^{-16}	1.22
5	3.50×10^{-14}	4.53×10^{-14}	0.773	2.02×10^{-15}	1.75×10^{-15}	1.16
10	5.69×10^{-14}	7.35×10^{-14}	0.774	3.48×10^{-15}	3.03×10^{-15}	1.15

Table 7: Beta dose rate coefficient comparison for individual tissues. Dose rate coefficients given in units of Gy Bq^{-1} s^{-1}.

	Breast			Trunk Muscle		
Energy (MeV)	**M. Coeff.**	**F. Coeff.**	**M/F**	**M. Coeff.**	**F. Coeff.**	**M/F**
0.1	1.66×10^{-17}	8.26×10^{-17}	0.201	4.28×10^{-23}	8.13×10^{-23}	0.526
0.5	2.02×10^{-17}	4.24×10^{-15}	0.00478	6.20×10^{-20}	4.12×10^{-19}	0.151
1	8.50×10^{-16}	3.58×10^{-14}	0.0237	3.07×10^{-20}	1.33×10^{-18}	0.0231
5	2.12×10^{-13}	4.09×10^{-13}	0.518	3.40×10^{-15}	1.14×10^{-16}	29.8
10	6.43×10^{-13}	8.25×10^{-13}	0.780	1.22×10^{-14}	8.41×10^{-16}	14.6

Comparison to the Radiological Accident in Gilan

Using the whole-body dose rate coefficients calculated above, comparisons are made to the doses reported in the IAEA's report for the radiological accident in Gilan. Using the whole-body dose rate coefficients, the whole-body dose, *D*, can be calculated for either photons or betas using the following equation:

$$D = At \sum_{j=E} \dot{D}_{C,j} i_j \tag{4}$$

where *t* is the time of exposure in seconds, *A* is the activity in Becquerels, $\dot{D}_{C,j}$ is the whole-body dose rate coefficient for each energy, *E*, emitted by the radioisotope, and i_j is the intensity of each energy in decimal form. This equation assumes that the time of exposure is much shorter than the half-life of the radioisotope and therefore the activity remains constant. The details given by the IAEA indicate the source was ^{192}Ir, the exposure time was 1.5 hours, and the activity of the source was 185 GBq (IAEA, 2002). The decay energies for ^{192}Ir are shown in Table 8. Using Equation 4 and the data in Table 8, the whole-body dose from photons is 0.3735 Gy and the whole-body dose from betas is 0.1733 Gy, for a total whole-body dose of 0.5468 Gy.

The analytical analysis provided by the IAEA assumed that 0.811 MeV was released per decay and that 30% of the source energy would be deposited resulting in 38.85 J of energy being deposited in the man involved in the accident (IAEA, 2002). The man's mass was 60 kg giving

him a whole-body dose of 0.6475 Gy. The total energy deposited in the 73 kg phantom from a 0.5468 Gy dose would be 39.91 J which is close to the IAEA's analytical estimation of energy deposited.

Based on biological dosimetry conducted after the accident, the whole-body dose was reported to be between 2.8 – 4.7 Gy (IAEA, 2002). The biological dosimetry was obtained using Dolphin's method (Dolphin, 1969) and greatly differs from the whole-body dose estimate calculated in this study. According to the IAEA, "the assumptions used to support [the biological dosimetry] models are sometimes debatable in their application to accident situations. Moreover, they assume a homogeneous exposure of the irradiated fraction of the body, which is rarely the case" (IAEA, 2002). To achieve a closer representation of a homogeneous exposure, new homogeneous whole-body dose rate coefficients were calculated using only energy deposited in the torso and head. These "modified torso dose rate coefficients" are provided in Appendix D. Using the modified torso dose rate coefficients with the method described above (new mass of

Table 8: Radiation emitted by ^{192}Ir (NNDC).

Photons Emitted			
Energy (MeV)	**Intensity (%)**	**Energy (MeV)**	**Intensity (%)**
0.31651	82.86	0.20579	3.131
0.46807	47.84	0.065122	2.65
0.30846	29.70	0.063001	2.07
0.29596	28.71	0.008910	1.50
0.60441	8.216	0.0614867	1.199
0.61246	5.34	0.07140	0.885
0.066832	4.54	0.37449	0.727
0.58858	4.522	0.20131	0.471
0.009440	3.92	0.48906	0.438
0.48458	3.91	0.28327	0.266
Betas Emitted			
Average Energy (MeV)	**Intensity (%)**	**Average Energy (MeV)**	**Intensity (%)**
0.20801	47.98	0.01972	0.1026
0.16032	41.42	0.01225	0.0059
0.07001	5.60	0.01813	0.0039

the male is 45 kg in this instance), the modified photon and beta doses were calculated to be 0.5868 Gy and 0.2796 Gy, respectively, for a total of 0.8664 Gy. While this dose estimate is higher it still is not consistent with biodosimetry estimations for whole-body dose.

The IAEA also reported that the man involved in the accident had a 3 cm × 3 cm skin desquamation on his right thigh implying that he received "contact with a point source with an estimated dose of 40 Gy" (IAEA, 2002). If the source was only contained in his breast pocket, it would not be expected for him to have received such a dose to his thigh. This suggests that the source was stored in his thigh pocket, at least for a short period, or he changed his body's geometry (i.e. sitting or leaning) enough to put the source closer to his thigh for a significant amount of time during his exposure.

Back Pocket Source

The plot of the whole-body dose rate coefficients for the photon and beta back pocket sources for the male and female phantoms are shown in Figure 7 (data in Appendix B). The photon coefficients follow a similar trend as the photon breast pocket source, however, the male coefficients are consistently about 0.85 – 0.90 times that of the female instead of the almost exact 1:1 ratio seen in the breast pocket scenario. The percent of energy deposited for photons is in the range of 14 – 24% for males above 70 keV and 13 – 23% for females above 70 keV.

The beta coefficients seem to follow a similar trend to the breast pocket beta source. The ratio of male-to-female coefficients ranges from about 0.75 – 0.85 for energies above 70 keV. Similar to the breast pocket source for betas, about 40 – 47% of the source energy is deposited in the body for all energies except the lowest energies (1 – 20 keV). As seen with the breast pocket source, the whole-body dose rate coefficients for photons and betas are approximately equal for source energies of about 30 to 40 keV.

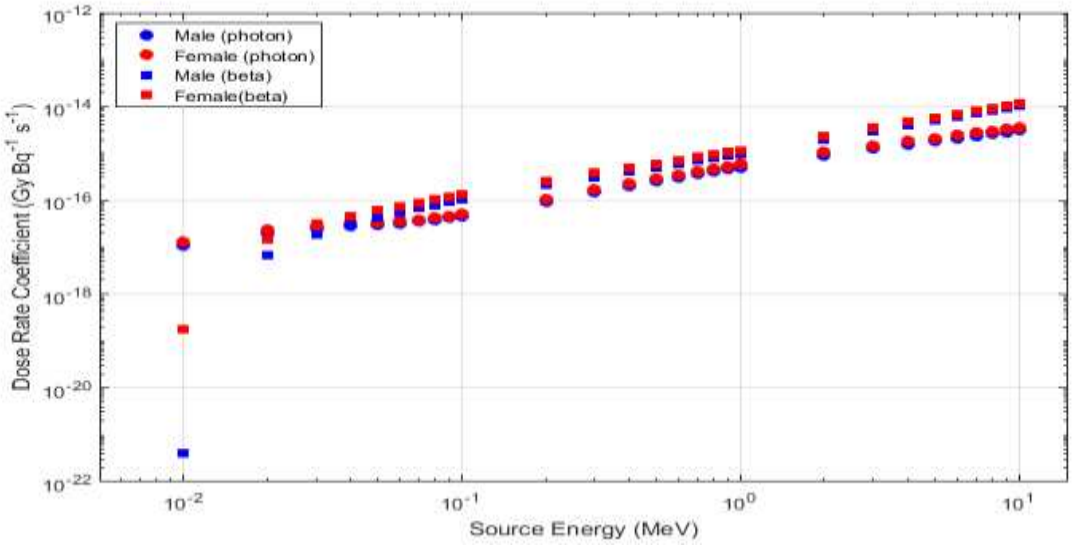

Figure 7: Plot of the whole-body dose rate coefficients for the male and female phantoms for photon and beta back pocket source.

Comparison to the Radiological Accident in Yanango

The estimated dose based on the whole-body dose rate coefficients for the Yanango accident is calculated using Equation 4, analogous to the approach used for the Gilan accident, but using the back pocket source geometry. The source was an ^{192}Ir source with an activity of 1.37 TBq, and the exposure time was 6.5 hours. The results are compared to the IAEA's accident report (IAEA, 2000). The patient's whole-body dose was estimated by the IAEA using a fluorescence in situ hybridization (FISH) technique (Darroudi and Natarajan, 2000). The FISH technique assumes a homogeneous whole-body exposure and is mostly practical for "low doses" (Darroudi and Natarajan, 2000). Using the FISH technique the whole-body dose was estimated to be 1.2 – 1.5 Gy (IAEA, 2000). Using the whole-body dose rate coefficients presented in Figures 8 and 9, the whole-body dose is calculated to be 13.12 Gy from photons and 2.59 Gy from betas for a total of 15.71 Gy. The whole-body dose calculated in this scenario, as in the Gilan scenario, is significantly different from the biodosimetry estimate provided in the IAEA's report. The differences in the estimates for whole-body doses for both scenarios indicate how

difficult it is to accurately estimate the whole-body dose when the parameters of the exposure scenario (time and geometry) are not well known.

Dose estimates provided for different organs in the report for the Yanango accident were obtained from Peruvian physicists at the Instituto Nacional de Enfermedades Neoplasicas (INEN) using the Prowess 3000 treatment planning computer system (IAEA, 2000). The organ doses calculated by INEN are compared to organ doses calculated using the organ dose rate coefficients for the individual organs calculated with MCNP6 and are presented in Table 9 (raw data in Appendix E).

The MCNP6 results for the gonads and bladder agree with the INEN results better than the femur and rectum results. The femur greatly varies but it is stated that INEN results were for a single point in the organ as opposed to the dose being calculated across the whole organ as was done with MCNP6. The dose would theoretically decrease in the femur as the distance from the source increases, thus reducing the average value of the dose to the whole organ. The general agreement between the two doses for the gonads and bladder seem to indicate that the dose-coefficients for individual organs calculated with MCNP6 may be a good estimate for retrospective analysis for organ doses. Organ doses were also calculated using Monte Carlo methods with a transport code MORSE (Multigroup Oak Ridge Stochastic Experiment) and a software package known as MDGE (Multidevice Graphics Editor) and reported by the IAEA. Using the MORSE code, the dose to the femur was estimated to be between 5 – 15 Gy which agrees much better with the dose calculated using the dose rate coefficients.

It is worth noting that the dose from betas is negligible (three orders of magnitude lower) or zero when calculating the organ doses for Table 9. It is also apparent, when comparing Tables 6 and 7 from the breast pocket source, that the beta whole-body dose rate coefficients were two or more

orders of magnitude lower than the photon whole-body dose rate coefficients also for most energies. This implies that beta dose is only of significant concern for skin and tissue just below the skin.

Table 9: Doses calculated by INEN and MCNP6.

Organ (Mass)	**INEN Dose (Gy)***	**MCNP6 Dose (Gy)**
Femur (786.53 g)	143	35.4
Gonads (17.5 g)	23	20.3
Bladder (13.92 g)	18	14.8
Rectum (29.98 g)	18	27.7
*Results taken from IAEA accident report (IAEA, 2000).		

Skin Dose

Skin dose rate coefficients are also calculated using MCNP6. The dose is calculated via two methods: (1) calculating fluence and subsequent conversion using ICRP 74 conversion coefficients for fluence to air kerma for photons and fluence to absorbed skin dose for betas and (2) calculating the energy deposited in the first 0.07 mm of skin. Both methods are calculated for a cylindrical volume of skin with a cross-sectional area of 10 cm^2 and a depth of 0.007 cm. In the model, the source was aligned with the center of the circular face of the model volume. This geometry ensures that the maximum skin dose for a 10 cm^2 area of skin is calculated because the absorbed dose will decrease as the radial distance from the source increases. MCNP6's output for method 1 is in Gray, but the output for method 2 is converted to Gray using the density (1.09 g cm^{-3}) and volume (10 cm^2 × 0.007 cm) of the skin with the following equation:

$$\text{Dose (Gy)} = \frac{E_D(1.602\times10^{-13}\ \text{J MeV}^{-1})(1000\ \text{g kg}^{-1})}{(1.09\ \text{g cm}^{-3})(10\ \text{cm}^2 \times 0.007\ \text{cm})} \quad (5)$$

The ICRP conversion coefficient for dose to air kerma is used assuming the kerma approximation was valid based on the data presented in Figure 5. The results for both methods for photons are plotted in Figure 8 (data in Appendix F). The calculated skin dose rate

coefficients for both methods are consistent, within 10% for each energy, with method 2 (the dose based on deposited energy) providing consistently higher results.

Using similar methods to calculate skin dose from betas proved more difficult with the chosen geometry. The shielding encapsulating the source blocks all betas with an energy less than 2.0 MeV from penetrating. The data collected are shown in Figure 9. The results from the two methods did not agree as well for betas as they did for photons, with Method 2 (the dose based on deposited energy) providing results 2-3 times higher. The discrepancy between the two methods is may be because the ICRP conversion factor assumes a whole-body homogeneous exposure. It is worth noting that none of the most common radiography sources (^{60}Co, ^{192}Ir, ^{75}Se, and ^{169}Yb) have average beta energies greater than 1 MeV, so it is unlikely that any of these sources, when shielded, would cause a significant beta dose to the skin. However, an unshielded beta source, as shown in the whole-body cases, will contribute significantly to the dose as most energy from betas is expected to be deposited in the skin.

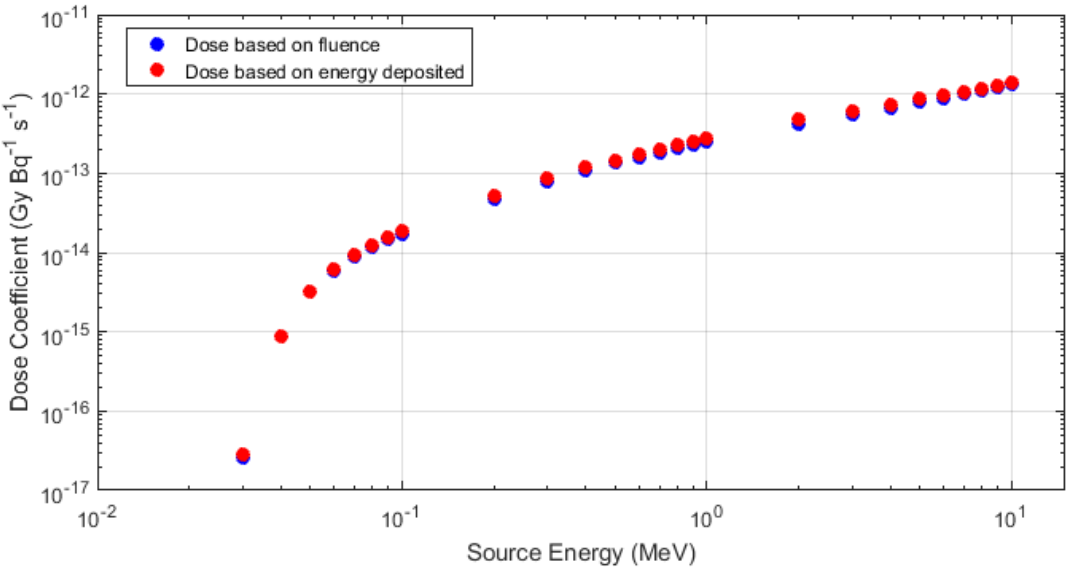

Figure 8: Plot of the dose rate coefficients for the skin dose for an encapsulated photon source.

Using the Method 2 skin dose rate coefficients, the skin dose for the Yanango incident is calculated using Equation 4 and compared to the INEN estimated skin dose of 9966 Gy (IAEA, 2000). The estimated skin dose for the Yanango accident is 7435 Gy based on the skin dose rate coefficients which is roughly 75% of the estimation by INEN, assuming there is no beta contribution to the dose. It is not clear from the IAEA report on what size area of skin the INEN dose is based, but if the skin dose is calculated with a smaller area of skin, then the INEN estimate indeed should be higher.

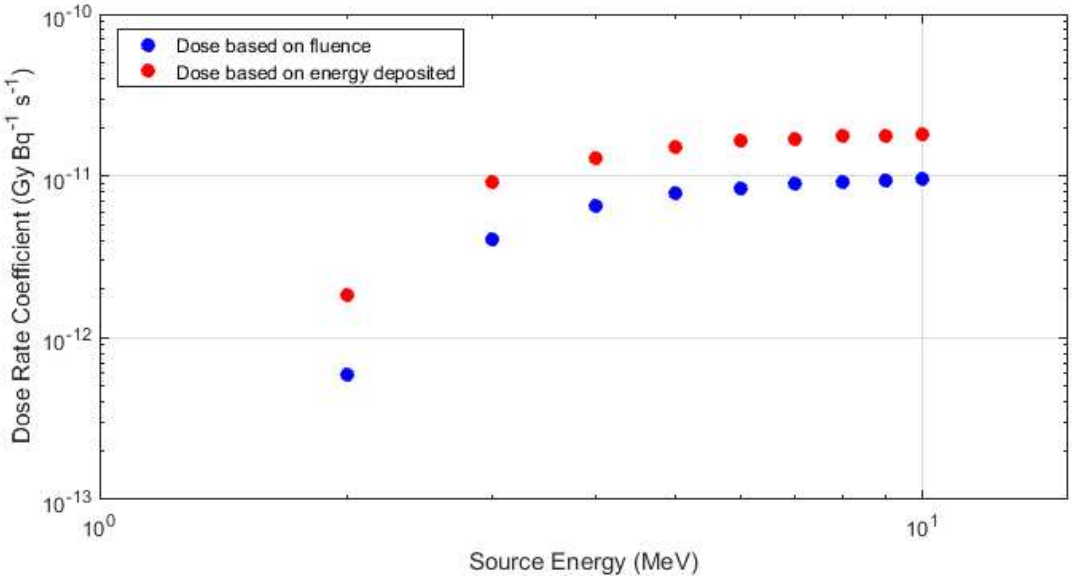

Figure 9: Plot of the dose rate coefficients for the skin dose for an encapsulated photon source.

Conclusions

Using dose rate coefficients to retrospectively assess the dose of a radiological accident, in theory, is a quick and accurate technique. However, the dose estimate is only as accurate as the information ascertained about the exposure scenario. Most information provided to retrospectively analyze a scenario is likely to be self-reported and can be un-reliable. Uncertainties in exposure time and geometry (movement of the source in pockets, moving the source from one pocket to another, handling of the source, etc.) can lead to uncertainties in the dose assessment. Unlike the ICRP conversion coefficients which have been published for a broad-beam, homogeneous, whole-body exposure to simplify geometries, the dose rate coefficients calculated in this study are trying to predict doses due to very particular geometries.

In general, the dose from the photons seem to influence whole-body and organ doses more than dose from beta particles. This is because the beta particles cannot penetrate as far as the photons can. However, a non-encapsulated beta source dose is expected to deliver a more significant dose to the skin.

The whole-body dose estimates calculated from the dose rate coefficients presented do not seem accurate when compared to the IAEA's published results from biodosimetry (0.5468 Gy vs. 2.8 Gy for the Gilan accident and 15.71 Gy vs. 1.5 Gy for the Yanango accident). The individual organ and skin doses calculated with their respective dose rate coefficients compared to the doses reported by the IAEA, retrospectively calculated also utilizing Monte Carlo methods, seem to be in closer agreement. It is clear, based on this study, biodosimetry and Monte Carlo methods seem to have discrepancies between them. This discrepancy is possibly due to the fact that biodosimetry assumes homogeneous exposures which is not the case for most accidental acute exposures.

Going forward, the method used in this study could be used for additional geometries (left breast pocket, left back pocket, and both side pant pockets) to calculate more dose rate coefficients. Skin dose coefficients for non-encapsulated photon and beta sources should also be calculated to see how significant beta dose would be to skin dose in that scenario. Combined with the coefficients presented in this study they could be used to more accurately assess a wide variety of acute dose exposures. Having coefficients to more rapidly compute doses may help predict how exposed individuals should be assessed following an acute radiation exposure.

While whole-body doses were used in this study to attempt to validate the method, the main concern following radiological accidents are doses to individual organs. A closer look at absorbed doses to specific organs (e.g. lungs, breast, gonads) and effective doses to those organs could provide further information what areas of the body take the most detriment from acute radiation exposures. The dose rate coefficients of this study are specifically for reference man and reference woman and thus are most accurate when using them for individuals similar to reference man and reference woman. Therefore, the method used in this study could be used to determine dose rate coefficients using geometries for different body sizes and types to see what effect they have on the organ doses.

References

10 C.F.R. § 20 (2017).

Bellamy, M.B. et al. (2016). Comparison of monoenergetic photon organ dose rate coefficients for stylized and voxel phantoms submerged in air. *Radiation Protection Dosimetry, 172* (4), 367-374.

Cember, H., and Johnson, T. E. (2009). *Introduction to Health Physics* (4th ed.). New York City, NY: McGraw Hill.

Darroudi F., Natarajan, A.T. (2000). Applications of FISH chromosome painting assay for dose reconstruction: state of art and current views. *Radiation Protection Dosimetry, 88,* 51-58.

Dolphin, G.W. (1969). Biological dosimetry with particular reference to chromosome aberration analysis a review of methods. In *Handling of Radiation Accidents (Proc. Int. Symp. Vienna, 1969) (*pp. 215-224). IAEA, Vienna.

Fisher, H. L. J. and Snyder, W. S. (1966). Variation of dose delivered by 137Cs as a function of body size from infancy to adulthood. *ORNL, 4007,* 221-228.

Hu, S. (2016). Linking doses with clinical scores of hematopoietic acute radiation syndrome. *Health Physics, 111*(4), 337-347.

International Atomic Energy Agency. (1998). Diagnosis and treatment of radiation injuries. *Safety Series, 2* (50).

International Atomic Energy Agency. (2000). *The Radiological Accident in Yanango*. Vienna: International Atomic Energy Agency.

International Atomic Energy Agency. (2002). *The Radiological Accident in Gilan*. Vienna: International Atomic Energy Agency.

International Commission on Radiological Protection. (1991). 1990 recommendations of the International Commission on Radiological Protection. *Annals of the ICRP, 21* (1-3).

International Commission on Radiological Protection. (1996). Conversion coefficients for use in radiological protection against external radiation. *Annals of the ICRP, 26* (3/4).

International Commission on Radiological Protection. (2002). Basic anatomical and physiological data for use in radiological protection: reference values. *Annals of the ICRP, 32* (3/4).

International Commission on Radiological Protection. (2007). The 2007 recommendations of the International Commission on Radiological Protection. *Annals of the ICRP, 37* (2-4).

International Commission on Radiological Protection. (2009). Adult reference computational phantoms. *Annals of the ICRP, 39* (2).

Johnson, T.E., and Birky, B.K. (2012). *Health Physics and Radiological Health.* Philadelphia: Wolters Kluwer Health.

McConn Jr, R.J. et al. (2011). *Compendium of Material Composition Data for Radiation Transport Modeling*. Richland, WA: Pacific Northwest National Laboratory.

National Nuclear Data Center. (n.d). Chart of nuclides. Retrieved December 1, 2016, from www.nndc.bnl.gov/chart

National Research Council. (2008). *Radiation Source Use and Replacement: Abbreviated Version*. National Academic Press.

Shultis, J. K. and Faw, R. E. (2000). *Radiation Shielding*. La Grange Park, IL: American Nuclear Society.

Sugarman, S. L. and Toohey, R. E. (2013). Practical medical applications of dose magnitude estimation. In *Medical Basis for Radiation-Accident Preparedness* (pp. 179-188). Oak Ridge, TN: Oak Ridge Associated Universities.

Turner, J. E. (2008). *Atoms, Radiation, and Radiation Protection* (3rd ed.). Wienheim: Wiley-VCH.

Veinot, K. G. and Hertel, N. E. (2007). Photon extremity absorbed dose and kerma conversion coefficients for calibration geometries. *Health Physics*, *92*(2), 179-185.

Xu, X. G. and Eckerman, K. F. (2010). *Handbook of Anatomical Models for Radiation Dosimetry.* Boca Raton, FL: CRC Press/Taylor & Francis Group.

Appendix A: Organ/Tissue Identification Numbers

Table A: Organ/Tissue Identification Numbers

ID/Cell	Organ/tissue	ID/Cell	Organ
1	Adrenal, left	45	Scapulae, cortical
2	Adrenal, right	46	Scapulae, spongiosa
3	Anterior nasal passage	47	Cervical spine, cortical
4	Posterior nasal passage down to larynx	48	Cervical spine, spongiosa
5	Oral mucosa, tongue	49	Thoracic spine, cortical
6	Oral mucosa, lips and cheeks	50	Thoracic spine, spongiosa
7	Trachea	51	Lumbar spine, cortical
8	Bronchi	52	Lumbar spine, spongiosa
9	Blood vessels, head	53	Sacrum, cortical
10	Blood vessels, trunks	54	Sacrum, spongiosa
11	Blood vessels, arms	55	Sternum, cortical
12	Blood vessels, legs	56	Sternum, spongiosa
13	Humeri, proximal end, cortical bone	57	Cartilage, head
14	Humeri, upper half, spongiosa	58	Cartilage, trunk
15	Humeri, upper half, medullary cavity	59	Cartilage, arms
16	Humeri, lower half, cortical	60	Cartilage, legs
17	Humeri, lower half, spongiosa	61	Brain
18	Humeri, lower half, medullary cavity	62	Breast, left, adipose tissue
19	Ulnae and radii, cortical	63	Breast, left, glandular tissue
20	Ulnae and radii, spongiosa	64	Breast, right, adipose tissue
21	Ulnae and radii, medullary cavity	65	Breast, right, glandular tissue
22	Wrists and hand bones, cortical	66	Eye lens, left
23	Wrists and hand bones, spongiosa	67	Eye bulb, left
24	Clavicles, cortical	68	Eye lens, right
25	Clavicles, spongiosa	69	Eye bulb, right
26	Cranium, cortical	70	Gall bladder wall
27	Cranium, spongiosa	71	Gall bladder contents
28	Femora, upper half, cortical	72	Stomach wall
29	Femora, upper half, spongiosa	73	Stomach contents
30	Femora, upper half, medullary cavity	74	Small intestine wall
31	Femora, lower half, cortical	75	Small intestine contents
32	Femora, lower half, spongiosa	76	Ascending colon wall
33	Femora, lower half, medullary cavity	77	Ascending colon contents
34	Tibiae, fibulae, and patellae, cortical	78	Transverse colon wall, right
35	Tibiae, fibulae, and patellae, spongiosa	79	Transverse colon contents, right
36	Tibiae, fibulae, and patellae, medullary cavity	80	Transverse colon wall, left
37	Ankles and foot bones, cortical	81	Transverse colon contents, left
38	Ankles and foot bones, spongiosa	82	Descending colon wall
39	Mandible, cortical	83	Descending colon contents
40	Mandible, spongiosa	84	Sigmoid colon wall
41	Pelvis, cortical	85	Sigmoid colon contents
42	Pelvis, spongiosa	86	Rectum wall
43	Ribs, cortical	87	Heart wall
44	Ribs, spongiosa	88	Heart contents (blood)

Table A (continued)

ID/Cell	Organ/tissue	ID/Cell	Organ
89	Kidney, left, cortex	115	Prostate
90	Kidney, left, medulla	116	Residual tissue, head
91	Kidney, left, pelvis	117	Residual tissue, trunk
92	Kidney, right, cortex	118	Residual tissue, arms
93	Kidney, right, medulla	119	Residual tissue, legs
94	Kidney, right, pelvis	120	Salivary glands, left
95	Liver	121	Salivary glands, right
96	Lungs, left, blood	122	Skin, head
97	Lungs, left, tissue	123	Skin, trunks
98	Lungs, right, blood	124	Skin, arms
99	Lungs, right, tissue	125	Skin, legs
100	Lymphatic nodes, ET airways	126	Spinal cord
101	Lymphatic nodes, thoracic airways	127	Spleen
102	Lymphatic nodes, head	128	Teeth
103	Lymphatic nodes, trunk	129	Testis, left
104	Lymphatic nodes, arms	130	Testis, right
105	Lymphatic nodes, legs	131	Thymus
106	Muscle, head	132	Thyroid
107	Muscle, trunk	133	Tongue (inner part)
108	Muscle, arms	134	Tonsils
109	Muscle, legs	135	Ureter, left
110	Oesophagus (wall)	136	Ureter, right
111	Ovary, left	137	Urinary bladder wall
112	Ovary, right	138	Urinary bladder contents
113	Pancreas	139	Uterus/cervix
114	Pituitary gland	140	Air inside body

Appendix B: Whole-Body Dose Rate Coefficient Data

Table B1: Dose data for photon breast pocket source

	Male			Female			
Source Energy (MeV)	**Energy Deposited (MeV)**	**% Deposited**	**Dose Rate Coefficient (Gy Bq^{-1} s^{-1})**	**Energy Deposited (MeV)**	**% Deposited**	**Dose Rate Coefficient (Gy Bq^{-1} s^{-1})**	**M/F D.R.C.**
0.001	0.00	-	-	0.00	-	-	-
0.01	0.004552	45.52	9.992×10^{-18}	0.004118	41.18	1.099×10^{-17}	0.9087
0.02	0.008089	40.44	1.775×10^{-17}	0.006955	34.77	1.857×10^{-17}	0.9561
0.03	0.01000	33.33	2.194×10^{-17}	0.008125	27.08	2.169×10^{-17}	1.012
0.04	0.01113	27.82	2.443×10^{-17}	0.008734	21.84	2.332×10^{-17}	1.047
0.05	0.01205	24.10	2.645×10^{-17}	0.009260	18.52	2.473×10^{-17}	1.070
0.06	0.01305	21.74	2.864×10^{-17}	0.009895	16.49	2.642×10^{-17}	1.084
0.07	0.01421	20.30	3.119×10^{-17}	0.01070	15.29	2.857×10^{-17}	1.092
0.08	0.01555	19.44	3.413×10^{-17}	0.01168	14.59	3.117×10^{-17}	1.095
0.09	0.01705	18.94	3.742×10^{-17}	0.01280	14.22	3.418×10^{-17}	1.095
0.1	0.01868	18.68	4.101×10^{-17}	0.01405	14.05	3.751×10^{-17}	1.093
0.2	0.03896	19.48	8.552×10^{-17}	0.03000	15.00	8.010×10^{-17}	1.068
0.3	0.06174	20.58	1.355×10^{-16}	0.04815	16.05	1.286×10^{-16}	1.054
0.4	0.08491	21.23	1.864×10^{-16}	0.06667	16.67	1.780×10^{-16}	1.047
0.5	0.1079	21.58	2.368×10^{-16}	0.08504	17.01	2.270×10^{-16}	1.043
0.6	0.1304	21.74	2.863×10^{-16}	0.1030	17.17	2.751×10^{-16}	1.041
0.7	0.1525	21.79	3.347×10^{-16}	0.1207	17.24	3.222×10^{-16}	1.039
0.8	0.1741	21.76	3.821×10^{-16}	0.1379	17.23	3.681×10^{-16}	1.038
0.9	0.1950	21.67	4.280×10^{-16}	0.1546	17.17	4.127×10^{-16}	1.037
1.0	0.2155	21.55	4.730×10^{-16}	0.1709	17.09	4.562×10^{-16}	1.037
2.0	0.3943	19.72	8.655×10^{-16}	0.3126	15.63	8.345×10^{-16}	1.037
3.0	0.5427	18.09	1.191×10^{-15}	0.4296	14.32	1.147×10^{-15}	1.039
4.0	0.6751	16.88	1.482×10^{-15}	0.5336	13.34	1.425×10^{-15}	1.040
5.0	0.7978	15.96	1.751×10^{-15}	0.6301	12.60	1.682×10^{-15}	1.041
6.0	0.9149	15.25	2.008×10^{-15}	0.7219	12.03	1.928×10^{-15}	1.042
7.0	1.029	14.69	2.258×10^{-15}	0.8111	11.59	2.166×10^{-15}	1.042
8.0	1.141	14.26	2.504×10^{-15}	0.8990	11.24	2.400×10^{-15}	1.043
9.0	1.251	13.90	2.746×10^{-15}	0.9853	10.95	2.631×10^{-15}	1.044
10.0	1.361	13.61	2.987×10^{-15}	1.071	10.71	2.861×10^{-15}	1.044

Table B2: Dose data for beta breast pocket source

	Male			Female			
Source Energy (MeV)	**Energy Deposited (MeV)**	**% Deposited**	**Dose Rate Coefficient (Gy Bq^{-1} s^{-1})**	**Energy Deposited (MeV)**	**% Deposited**	**Dose Rate Coefficient (Gy Bq^{-1} s^{-1})**	**M/F D.R.C.**
0.001	0.00	-	-	0.00	-	-	-
0.01	0.00004708	0.4708	1.033×10^{-19}	0.00008130	0.8130	2.171×10^{-19}	0.4761
0.02	0.005118	25.59	1.123×10^{-17}	0.005328	26.64	1.423×10^{-17}	0.7897
0.03	0.01100	36.65	2.413×10^{-17}	0.01077	35.89	2.875×10^{-17}	0.8394
0.04	0.01660	41.49	3.643×10^{-17}	0.01568	39.21	4.188×10^{-17}	0.8699
0.05	0.02206	44.12	4.842×10^{-17}	0.02020	40.40	5.394×10^{-17}	0.8977
0.06	0.02729	45.48	5.989×10^{-17}	0.02452	40.87	6.548×10^{-17}	0.9147
0.07	0.03240	46.28	7.111×10^{-17}	0.02881	41.16	7.693×10^{-17}	0.9244
0.08	0.03739	46.74	8.207×10^{-17}	0.03301	41.26	8.813×10^{-17}	0.9313
0.09	0.04237	47.08	9.301×10^{-17}	0.03732	41.47	9.965×10^{-17}	0.9333
0.1	0.04728	47.28	1.038×10^{-16}	0.04176	41.76	1.115×10^{-16}	0.9307
0.2	0.09297	46.49	2.041×10^{-16}	0.08609	43.04	2.299×10^{-16}	0.8878
0.3	0.1343	44.76	2.947×10^{-16}	0.1239	41.29	3.307×10^{-16}	0.8911
0.4	0.1742	43.56	3.825×10^{-16}	0.1603	40.08	4.280×10^{-16}	0.8936
0.5	0.2144	42.88	4.705×10^{-16}	0.1965	39.31	5.248×10^{-16}	0.8967
0.6	0.2545	42.42	5.586×10^{-16}	0.2324	38.73	6.204×10^{-16}	0.9004
0.7	0.2946	42.09	6.467×10^{-16}	0.2678	38.26	7.151×10^{-16}	0.9044
0.8	0.3347	41.83	7.346×10^{-16}	0.3030	37.88	8.091×10^{-16}	0.9079
0.9	0.3745	41.61	8.220×10^{-16}	0.3380	37.56	9.025×10^{-16}	0.9109
1.0	0.4142	41.42	9.091×10^{-16}	0.3728	37.28	9.955×10^{-16}	0.9132
2.0	0.8105	40.53	1.779×10^{-15}	0.7269	36.35	1.941×10^{-15}	0.9166
3.0	1.217	40.55	2.670×10^{-15}	1.086	36.21	2.900×10^{-15}	0.9207
4.0	1.628	40.70	3.573×10^{-15}	1.442	36.05	3.850×10^{-15}	0.9281
5.0	2.044	40.87	4.486×10^{-15}	1.793	35.86	4.787×10^{-15}	0.9371
6.0	2.459	40.99	5.398×10^{-15}	2.138	35.63	5.707×10^{-15}	0.9459
7.0	2.874	41.06	6.309×10^{-15}	2.479	35.41	6.619×10^{-15}	0.9532
8.0	3.285	41.07	7.211×10^{-15}	2.816	35.20	7.518×10^{-15}	0.9592
9.0	3.697	41.07	8.114×10^{-15}	3.151	35.01	8.413×10^{-15}	0.9645
10.0	4.105	41.05	9.010×10^{-15}	3.483	34.83	9.300×10^{-15}	0.9688

Table B3: Dose data for photon back pocket source

	Male			Female			
Source Energy (MeV)	**Energy Deposited (MeV)**	**% Deposited**	**Dose Rate Coefficient (Gy Bq^{-1} s^{-1})**	**Energy Deposited (MeV)**	**% Deposited**	**Dose Rate Coefficient (Gy Bq^{-1} s^{-1})**	**M/F D.R.C.**
0.001	0.00	-	0	0.00	-	0	-
0.01	0.004969	49.69	1.091×10^{-17}	0.004861	48.61	1.298×10^{-17}	0.8401
0.02	0.009125	45.62	2.002×10^{-17}	0.008793	43.96	2.348×10^{-17}	0.8530
0.03	0.01154	38.45	2.532×10^{-17}	0.01082	36.07	2.889×10^{-17}	0.8763
0.04	0.01284	32.10	2.818×10^{-17}	0.01184	29.59	3.160×10^{-17}	0.8918
0.05	0.01381	27.62	3.031×10^{-17}	0.01265	25.31	3.379×10^{-17}	0.8970
0.06	0.01485	24.76	3.260×10^{-17}	0.01360	22.67	3.631×10^{-17}	0.8976
0.07	0.01609	22.99	3.531×10^{-17}	0.01476	21.09	3.941×10^{-17}	0.8960
0.08	0.01754	21.93	3.850×10^{-17}	0.01614	20.17	4.309×10^{-17}	0.8934
0.09	0.01917	21.30	4.207×10^{-17}	0.01770	19.66	4.725×10^{-17}	0.8905
0.1	0.02097	20.97	4.601×10^{-17}	0.01941	19.41	5.182×10^{-17}	0.8879
0.2	0.04317	21.58	9.473×10^{-17}	0.04063	20.32	1.085×10^{-16}	0.8731
0.3	0.06789	22.63	1.490×10^{-16}	0.06428	21.43	1.716×10^{-16}	0.8680
0.4	0.09289	23.22	2.038×10^{-16}	0.08821	22.05	2.355×10^{-16}	0.8655
0.5	0.1175	23.51	2.580×10^{-16}	0.1118	22.37	2.986×10^{-16}	0.8638
0.6	0.1417	23.61	3.109×10^{-16}	0.1350	22.49	3.603×10^{-16}	0.8627
0.7	0.1652	23.60	3.625×10^{-16}	0.1575	22.50	4.205×10^{-16}	0.8620
0.8	0.1881	23.51	4.128×10^{-16}	0.1795	22.43	4.792×10^{-16}	0.8615
0.9	0.2103	23.37	4.615×10^{-16}	0.2008	22.31	5.360×10^{-16}	0.8610
1.0	0.2320	23.20	5.092×10^{-16}	0.2216	22.16	5.915×10^{-16}	0.8608
2.0	0.4203	21.02	9.22×10^{-16}	0.4016	20.08	1.072×10^{-15}	0.8602
3.0	0.5757	19.19	1.263×10^{-15}	0.5497	18.32	1.468×10^{-15}	0.8608
4.0	0.7140	17.85	1.567×10^{-15}	0.6812	17.03	1.819×10^{-15}	0.8615
5.0	0.8421	16.84	1.848×10^{-15}	0.8027	16.05	2.143×10^{-15}	0.8623
6.0	0.9642	16.07	2.116×10^{-15}	0.9182	15.30	2.452×10^{-15}	0.8631
7.0	1.083	15.47	2.376×10^{-15}	1.030	14.72	$2.751 \times 10^{-15`}$	0.8639
8.0	1.200	15.00	2.633×10^{-15}	1.140	14.26	3.045×10^{-15}	0.8646
9.0	1.315	14.61	2.885×10^{-15}	1.249	13.88	3.335×10^{-15}	0.8651
10.0	1.429	14.29	3.136×10^{-15}	1.357	13.57	3.623×10^{-15}	0.8656

Table B4: Dose data for beta back pocket source

	Male			Female			
Source Energy (MeV)	**Energy Deposited (MeV)**	**% Deposited**	**Dose Rate Coefficient (Gy Bq^{-1} s^{-1})**	**Energy Deposited (MeV)**	**% Deposited**	**Dose Rate Coefficient (Gy Bq^{-1} s^{-1})**	**M/F D.R.C.**
0.001	0.00	-	-	0.00	-	-	-
0.01	0.0000001873	0.001873	4.109×10^{-22}	0.00006523	0.6523	1.742×10^{-19}	0.002359
0.02	0.003020	15.10	6.627×10^{-18}	0.005549	27.75	1.482×10^{-17}	0.4473
0.03	0.008412	28.04	1.846×10^{-17}	0.01174	39.13	3.134×10^{-17}	0.5889
0.04	0.01414	35.34	3.102×10^{-17}	0.01736	43.40	4.635×10^{-17}	0.6694
0.05	0.01984	39.68	4.353×10^{-17}	0.02269	45.37	6.05×10^{-17}	0.7187
0.06	0.02542	42.36	5.578×10^{-17}	0.02791	46.52	7.453×10^{-17}	0.7484
0.07	0.03091	44.16	6.783×10^{-17}	0.03317	47.38	8.855×10^{-17}	0.7660
0.08	0.03630	45.38	7.967×10^{-17}	0.03841	48.01	1.026×10^{-16}	0.7768
0.09	0.04167	46.30	9.144×10^{-17}	0.04370	48.56	1.167×10^{-16}	0.7836
0.1	0.04709	47.09	1.033×10^{-16}	0.04897	48.97	1.307×10^{-16}	0.7904
0.2	0.09763	48.81	2.142×10^{-16}	0.09799	48.99	2.616×10^{-16}	0.8189
0.3	0.1435	47.85	3.150×10^{-16}	0.1429	47.64	3.816×10^{-16}	0.8254
0.4	0.1873	46.82	4.110×10^{-16}	0.1856	46.39	4.955×10^{-16}	0.8295
0.5	0.2301	46.02	5.050×10^{-16}	0.2277	45.53	6.079×10^{-16}	0.8308
0.6	0.2729	45.49	5.989×10^{-16}	0.2698	44.97	7.204×10^{-16}	0.8313
0.7	0.3159	45.12	6.932×10^{-16}	0.3122	44.60	8.336×10^{-16}	0.8316
0.8	0.3590	44.87	7.878×10^{-16}	0.3548	44.35	9.473×10^{-16}	0.8316
0.9	0.4022	44.68	8.825×10^{-16}	0.3976	44.18	1.062×10^{-15}	0.8314
1.0	0.4155	41.55	9.776×10^{-16}	0.4404	44.04	1.176×10^{-15}	0.8313
2.0	0.8906	44.53	1.954×10^{-15}	0.8734	43.67	2.332×10^{-15}	0.8380
3.0	1.352	45.06	2.967×10^{-15}	1.312	43.73	3.503×10^{-15}	0.8469
4.0	1.820	45.49	3.993×10^{-15}	1.751	43.77	4.674×10^{-15}	0.8543
5.0	2.294	45.89	5.035×10^{-15}	2.193	43.86	5.855×10^{-15}	0.8600
6.0	2.770	46.16	6.078×10^{-15}	2.636	43.93	7.038×10^{-15}	0.8636
7.0	3.246	46.37	7.123×10^{-15}	3.083	44.04	8.231×10^{-15}	0.8653
8.0	3.719	46.49	8.162×10^{-15}	3.532	44.14	9.429×10^{-15}	0.8656
9.0	4.195	46.62	9.207×10^{-15}	3.986	44.29	1.064×10^{-14}	0.8652
10.0	4.670	46.70	1.025×10^{-14}	4.441	44.41	1.186×10^{-14}	0.8643

Appendix C: Data for Breast and Trunk Tissue Example

Table C1: photon breast pocket source data used to calculate the dose rate coefficients for the reference male breast (mass 0.02498 kg)

	Energy Deposited in Cell: (MeV)				
Source Energy (MeV)	**62**	**63**	**64**	**65**	**Total Energy Deposited (MeV)**
0.1	9.10×10^{-5}	5.09×10^{-5}	1.71×10^{-6}	1.01×10^{-6}	1.45×10^{-4}
0.5	5.62×10^{-4}	3.16×10^{-4}	1.42×10^{-5}	8.92×10^{-6}	9.00×10^{-4}
1.0	1.06×10^{-3}	5.96×10^{-4}	3.10×10^{-5}	1.97×10^{-5}	1.71×10^{-3}
5.0	3.36×10^{-3}	1.89×10^{-3}	1.29×10^{-4}	8.57×10^{-5}	5.46×10^{-3}
10.0	5.44×10^{-3}	3.07×10^{-3}	2.25×10^{-4}	1.47×10^{-4}	8.88×10^{-3}

Table C2: Photon breast pocket source data used to calculate dose rate coefficients for the reference male trunk muscle (cell 107, mass 15.00682 kg)

Source Energy (MeV)	Energy Deposited (MeV)
0.1	4.11×10^{-3}
0.5	2.47×10^{-2}
1.0	5.01×10^{-2}
5.0	1.89×10^{-1}
10.0	3.26×10^{-1}

Table C3: Photon breast pocket source data used to calculate dose rate coefficients for the reference female breast (mass 0.50002 kg)

	Energy Deposited in Cell: (MeV)				
Source Energy (MeV)	**62**	**63**	**64**	**65**	**Total Energy Deposited (MeV)**
0.1	1.37×10^{-3}	2.18×10^{-3}	1.18×10^{-4}	6.28×10^{-5}	3.73×10^{-3}
0.5	8.79×10^{-3}	1.36×10^{-2}	7.96×10^{-4}	4.23×10^{-4}	2.36×10^{-2}
1.0	1.68×10^{-2}	2.56×10^{-2}	1.54×10^{-3}	8.32×10^{-4}	4.47×10^{-2}
5.0	5.36×10^{-2}	8.01×10^{-2}	5.07×10^{-3}	2.81×10^{-3}	1.42×10^{-1}
10.0	8.68×10^{-2}	1.30×10^{-1}	8.24×10^{-3}	4.62×10^{-3}	2.29×10^{-1}

Table C4: Photon breast pocket source data used to calculate dose rate coefficients for the reference female trunk muscle (cell 107, mass 8.51822 kg)

Source Energy (MeV)	Energy Deposited (MeV)
0.1	1.76×10^{-3}
0.5	1.11×10^{-2}
1.0	2.33×10^{-2}
5.0	9.29×10^{-2}
10.0	1.61×10^{-1}

Table C5: Electron breast pocket source data used to calculate dose rate coefficients for the reference male breast (mass 0.02498 kg)

	Energy Deposited in Cell: (MeV)				
Source Energy (MeV)	**62**	**63**	**64**	**65**	**Total Energy Deposited (MeV)**
0.1	2.71×10^{-7}	2.32×10^{-6}	8.09×10^{-10}	0	2.59×10^{-6}
0.5	1.08×10^{-7}	2.88×10^{-6}	7.15×10^{-8}	9.16×10^{-8}	3.15×10^{-6}
1.0	6.30×10^{-5}	6.94×10^{-5}	4.88×10^{-8}	8.53×10^{-8}	1.33×10^{-4}
5.0	2.44×10^{-2}	8.59×10^{-3}	1.15×10^{-6}	1.57×10^{-7}	3.30×10^{-2}
10.0	6.59×10^{-2}	3.43×10^{-2}	3.19×10^{-5}	6.14×10^{-6}	1.00×10^{-1}

Table C6: Electron breast pocket source data used to calculate dose rate coefficients for the reference male trunk muscle (cell 107, mass 15.00682 kg)

Source Energy (MeV)	Energy Deposited (MeV)
0.1	4.01×10^{-9}
0.5	5.81×10^{-6}
1.0	2.87×10^{-6}
5.0	3.19×10^{-1}
10.0	1.15×10^{0}

Table C7: Electron breast pocket source data used to calculate dose rate coefficients for the reference female breast (mass 0.50002 kg)

	Energy Deposited in Cell: (MeV)				
Source Energy (MeV)	**62**	**63**	**64**	**65**	**Total Energy Deposited (MeV)**
0.1	4.17×10^{-5}	2.07×10^{-4}	9.21×10^{-6}	4.29×10^{-8}	2.58×10^{-4}
0.5	7.64×10^{-5}	1.30×10^{-2}	1.75×10^{-4}	4.42×10^{-6}	1.32×10^{-2}
1.0	4.64×10^{-3}	1.07×10^{-1}	5.54×10^{-4}	1.99×10^{-5}	1.12×10^{-1}
5.0	3.48×10^{-1}	9.20×10^{-1}	6.77×10^{-3}	2.22×10^{-3}	1.28×10^{0}
10.0	8.35×10^{-1}	1.71×10^{0}	2.00×10^{-2}	9.41×10^{-3}	2.57×10^{0}

Table C8: Electron breast pocket source data used to calculate dose rate coefficients for the reference female trunk muscle (cell 107, mass 8.51822 kg)

Source Energy (MeV)	Energy Deposited (MeV)
0.1	4.33×10^{-9}
0.5	2.19×10^{-5}
1.0	7.07×10^{-5}
5.0	6.08×10^{-3}
10.0	4.47×10^{-2}

Appendix D: Modified Dose Rate Coefficient Data

Table D1: "Modified" dose data for photon breast pocket source

Source Energy (MeV)	Energy Deposited (MeV)	% Deposited	Dose Coefficient (Gy Bq^{-1} s^{-1})
0.001	0.00	-	-
0.01	0.004550	45.50	1.620×10^{-17}
0.02	0.008080	40.40	2.876×10^{-17}
0.03	0.009950	33.17	3.542×10^{-17}
0.04	0.01098	27.46	3.910×10^{-17}
0.05	0.01180	23.61	4.202×10^{-17}
0.06	0.01272	21.19	4.527×10^{-17}
0.07	0.01381	19.73	4.917×10^{-17}
0.08	0.1510	18.87	5.374×10^{-17}
0.09	0.01654	18.38	5.889×10^{-17}
0.1	0.01813	18.13	5.453×10^{-17}
0.2	0.03780	18.90	1.346×10^{-16}
0.3	0.05981	19.94	2.129×10^{-16}
0.4	0.08211	20.53	2.923×10^{-16}
0.5	0.1042	20.83	3.708×10^{-16}
0.6	0.1257	20.96	4.477×10^{-16}
0.7	0.1468	20.97	5.227×10^{-16}
0.8	0.1674	20.92	5.959×10^{-16}
0.9	0.1873	20.81	6.667×10^{-16}
1.0	0.2067	20.67	7.360×10^{-16}
2.0	0.3754	18.77	1.336×10^{-15}
3.0	0.5142	17.14	1.831×10^{-15}
4.0	0.6376	15.94	2.270×10^{-15}
5.0	0.7518	15.04	2.677×10^{-15}
6.0	0.8607	14.34	3.064×10^{-15}
7.0	0.9663	13.80	3.440×10^{-15}
8.0	1.070	13.38	3.811×10^{-15}
9.0	1.173	13.03	4.175×10^{-15}
10.0	1.275	12.75	4.538×10^{-15}

Table D2: "Modified" dose data for beta breast pocket source

Source Energy (MeV)	Energy Deposited (MeV)	% Deposited	Dose Coefficient (Gy Bq^{-1} s^{-1})
0.001	0.00	-	-
0.01	0.00004708	0.4708	1.676×10^{-19}
0.02	0.005118	25.59	1.822×10^{-17}
0.03	0.01100	36.65	3.914×10^{-17}
0.04	0.01660	41.49	5.909×10^{-17}
0.05	0.02206	44.12	7.853×10^{-17}
0.06	0.02729	45.48	9.714×10^{-17}
0.07	0.03240	46.28	1.153×10^{-16}
0.08	0.03739	46.74	1.331×10^{-16}
0.09	0.04237	47.08	1.508×10^{-16}
0.1	0.04728	47.28	1.683×10^{-16}
0.2	0.09244	46.22	3.291×10^{-16}
0.3	0.1334	44.47	4.749×10^{-16}
0.4	0.1731	43.27	6.162×10^{-16}
0.5	0.2131	42.63	7.588×10^{-16}
0.6	0.2533	42.22	9.018×10^{-16}
0.7	0.2936	41.94	1.045×10^{-15}
0.8	0.3337	41.72	1.188×10^{-15}
0.9	0.3737	41.52	1.330×10^{-15}
1.0	0.4135	41.35	1.472×10^{-15}
2.0	0.8102	40.51	2.884×10^{-15}
3.0	1.216	40.55	4.330×10^{-15}
4.0	1.628	40.69	5.794×10^{-15}
5.0	2.044	40.87	7.275×10^{-15}
6.0	2.459	40.99	8.755×10^{-15}
7.0	2.874	41.06	1.023×10^{-14}
8.0	3.285	41.06	1.169×10^{-14}
9.0	3.696	41.07	1.316×10^{-14}
10.0	4.104	41.04	1.461×10^{-14}

Appendix E: Organ Data for Yanango Comparison

Table E1: Photon back source data used to calculate doses to the male femur (total mass of 1.57306 kg)

	Energy Deposited in Cells: (MeV)					
Source Energy (MeV)	**28**	**29**	**30**	**31**	**32**	**33**
0.001	0	0	0	0	0	0
0.01	0	0	0	0	0	0
0.02	3.09×10^{-6}	6.42×10^{-7}	8.04×10^{-10}	6.12×10^{-8}	1.13×10^{-8}	0
0.03	1.20×10^{-4}	4.14×10^{-5}	2.78×10^{-7}	4.26×10^{-6}	5.95×10^{-7}	1.02×10^{-7}
0.04	3.27×10^{-4}	1.20×10^{-4}	1.43×10^{-6}	2.52×10^{-5}	3.02×10^{-6}	8.71×10^{-7}
0.05	4.65×10^{-4}	1.80×10^{-4}	3.01×10^{-6}	5.16×10^{-5}	6.28×10^{-6}	2.21×10^{-6}
0.06	5.31×10^{-4}	2.22×10^{-4}	4.52×10^{-6}	7.18×10^{-5}	9.22×10^{-6}	3.77×10^{-6}
0.07	5.57×10^{-4}	2.53×10^{-4}	5.97×10^{-6}	8.56×10^{-5}	1.18×10^{-5}	5.23×10^{-6}
0.08	5.64×10^{-4}	2.80×10^{-4}	7.36×10^{-6}	9.42×10^{-5}	1.41×10^{-5}	6.75×10^{-6}
0.09	5.63×10^{-4}	3.06×10^{-4}	8.81×10^{-6}	9.98×10^{-5}	1.60×10^{-5}	8.37×10^{-6}
0.1	5.59×10^{-4}	3.33×10^{-4}	1.02×10^{-5}	1.05×10^{-4}	1.77×10^{-5}	9.97×10^{-6}
0.2	5.92×10^{-4}	6.39×10^{-4}	2.57×10^{-5}	1.33×10^{-4}	3.88×10^{-5}	2.81×10^{-5}
0.3	7.17×10^{-4}	9.76×10^{-4}	4.23×10^{-5}	1.72×10^{-4}	6.68×10^{-5}	4.90×10^{-5}
0.4	8.73×10^{-4}	1.32×10^{-3}	5.81×10^{-5}	2.19×10^{-4}	1.00×10^{-4}	7.10×10^{-5}
0.5	1.04×10^{-3}	1.66×10^{-3}	7.47×10^{-5}	2.69×10^{-4}	1.37×10^{-4}	9.33×10^{-5}
0.6	1.21×10^{-3}	1.99×10^{-3}	9.01×10^{-5}	3.22×10^{-4}	1.76×10^{-4}	1.15×10^{-4}
0.7	1.37×10^{-3}	2.31×10^{-3}	1.06×10^{-4}	3.77×10^{-4}	2.17×10^{-4}	1.38×10^{-4}
0.8	1.54×10^{-3}	2.62×10^{-3}	1.20×10^{-4}	4.33×10^{-4}	2.58×10^{-4}	1.61×10^{-4}
0.9	1.70×10^{-3}	3.93×10^{-3}	1.36×10^{-4}	4.87×10^{-4}	3.01×10^{-4}	1.82×10^{-4}
1.0	1.86×10^{-3}	3.23×10^{-3}	1.50×10^{-4}	5.41×10^{-4}	3.45×10^{-4}	2.05×10^{-4}
2.0	3.28×10^{-3}	5.81×10^{-3}	2.78×10^{-4}	1.06×10^{-3}	7.80×10^{-4}	4.08×10^{-4}
3.0	4.51×10^{-3}	7.94×10^{-3}	3.86×10^{-4}	1.53×10^{-3}	1.18×10^{-3}	5.79×10^{-4}
4.0	5.66×10^{-3}	9.82×10^{-3}	4.77×10^{-4}	1.96×10^{-3}	1.55×10^{-3}	7.35×10^{-4}
5.0	6.77×10^{-3}	1.16×10^{-2}	5.62×10^{-4}	2.39×10^{-3}	1.90×10^{-3}	8.74×10^{-4}
6.0	7.87×10^{-3}	1.32×10^{-2}	6.43×10^{-4}	2.83×10^{-3}	2.23×10^{-3}	1.01×10^{-3}
7.0	8.97×10^{-3}	1.48×10^{-2}	7.18×10^{-4}	3.26×10^{-3}	2.55×10^{-3}	1.14×10^{-3}
8.0	1.01×10^{-2}	1.64×10^{-2}	7.88×10^{-4}	3.68×10^{-3}	2.86×10^{-3}	1.26×10^{-3}
9.0	1.12×10^{-2}	1.79×10^{-2}	8.60×10^{-4}	4.11×10^{-3}	3.17×10^{-3}	1.38×10^{-3}
10.0	1.24×10^{-2}	1.95×10^{-2}	9.29×10^{-4}	4.55×10^{-3}	3.48×10^{-3}	1.50×10^{-3}

Table E2: Photon back source data used to calculate doses to the reference man's rectum (cell 86, mass of 0.02998 kg), gonads (cells 129 and 130, total mass of 0.035 kg), and bladder (cell 137, mass of 0.05001 kg)

	Energy Deposited in Cells: (MeV)			
Source Energy (MeV)	**86**	**129**	**130**	**137**
0.001	0	0	0	0
0.01	0	9.55×10^{-12}	1.92×10^{-11}	0
0.02	3.85×10^{-8}	1.12×10^{-8}	1.27×10^{-8}	3.31×10^{-9}
0.03	2.38×10^{-6}	7.34×10^{-7}	1.04×10^{-6}	6.97×10^{-7}
0.04	6.55×10^{-6}	2.28×10^{-6}	3.15×10^{-6}	3.09×10^{-6}
0.05	9.78×10^{-6}	3.59×10^{-6}	4.82×10^{-6}	5.99×10^{-6}
0.06	1.20×10^{-5}	4.58×10^{-6}	5.98×10^{-6}	8.58×10^{-6}
0.07	1.39×10^{-5}	5.33×10^{-6}	6.84×10^{-6}	1.07×10^{-5}
0.08	1.55×10^{-5}	6.00×10^{-6}	7.66×10^{-6}	1.26×10^{-5}
0.09	1.71×10^{-5}	6.57×10^{-6}	8.45×10^{-6}	1.43×10^{-5}
0.1	1.89×10^{-5}	7.21×10^{-6}	9.17×10^{-6}	1.60×10^{-5}
0.2	3.80×10^{-5}	1.40×10^{-5}	1.77×10^{-5}	3.33×10^{-5}
0.3	5.91×10^{-5}	2.25×10^{-5}	2.77×10^{-5}	5.23×10^{-5}
0.4	8.04×10^{-5}	3.10×10^{-5}	3.78×10^{-5}	7.23×10^{-5}
0.5	1.02×10^{-4}	3.97×10^{-5}	4.80×10^{-5}	9.18×10^{-5}
0.6	1.23×10^{-4}	4.84×10^{-5}	5.83×10^{-5}	1.12×10^{-4}
0.7	1.44×10^{-4}	5.62×10^{-5}	6.75×10^{-5}	1.31×10^{-4}
0.8	1.64×10^{-4}	6.50×10^{-5}	7.71×10^{-5}	1.51×10^{-4}
0.9	1.84×10^{-4}	7.32×10^{-5}	8.69×10^{-5}	1.69×10^{-4}
1.0	2.03×10^{-4}	8.05×10^{-5}	9.64×10^{-5}	1.87×10^{-4}
2.0	3.72×10^{-4}	1.52×10^{-4}	1.77×10^{-4}	3.53×10^{-4}
3.0	5.10×10^{-4}	2.09×10^{-4}	2.44×10^{-4}	4.92×10^{-4}
4.0	6.32×10^{-4}	2.60×10^{-4}	3.03×10^{-4}	6.20×10^{-4}
5.0	7.44×10^{-4}	3.09×10^{-4}	3.56×10^{-4}	7.40×10^{-4}
6.0	8.55×10^{-4}	3.55×10^{-4}	4.13×10^{-4}	8.56×10^{-4}
7.0	9.59×10^{-4}	4.00×10^{-4}	4.63×10^{-4}	9.64×10^{-4}
8.0	1.07×10^{-3}	4.45×10^{-4}	5.19×10^{-4}	1.07×10^{-3}
9.0	1.17×10^{-3}	4.88×10^{-4}	5.68×10^{-4}	1.17×10^{-3}
10.0	1.28×10^{-3}	5.31×10^{-4}	6.19×10^{-4}	1.28×10^{-3}

Appendix F: Skin Dose Data

Table F1: Photon data for skin dose rate coefficients

Source Energy	Method 1 Dose Rate Coefficient (Gy Bq^{-1} s^{-1})	Method 2 Energy Deposited (MeV)	Method 2 Dose Rate Coefficient (Gy Bq^{-1} s^{-1})	Ratio
0.01	0	0	0	-
0.02	0	0	0	-
0.03	2.551×10^{-17}	1.352×10^{-8}	2.838×10^{-17}	0.8988
0.04	8.631×10^{-16}	4.218×10^{-7}	8.856×10^{-16}	0.9747
0.05	3.152×10^{-15}	1.552×10^{-6}	3.258×10^{-15}	0.9674
0.06	5.906×10^{-15}	2.944×10^{-6}	6.181×10^{-15}	0.9554
0.07	8.959×10^{-15}	4.385×10^{-6}	9.207×10^{-15}	0.9731
0.08	1.157×10^{-14}	5.875×10^{-6}	1.234×10^{-14}	0.9376
0.09	1.460×10^{-14}	7.345×10^{-6}	1.542×10^{-14}	0.9467
0.1	1.741×10^{-14}	8.910×10^{-6}	1.871×10^{-14}	0.9303
0.2	4.806×10^{-14}	2.493×10^{-5}	5.235×10^{-14}	0.9181
0.3	7.810×10^{-14}	4.067×10^{-5}	8.539×10^{-14}	0.9147
0.4	1.068×10^{-13}	5.578×10^{-5}	1.171×10^{-13}	0.9120
0.5	1.342×10^{-13}	6.990×10^{-5}	1.468×10^{-13}	0.9147
0.6	1.600×10^{-13}	8.329×10^{-5}	1.749×10^{-13}	0.9150
0.7	1.840×10^{-13}	9.638×10^{-5}	2.024×10^{-13}	0.9092
0.8	2.076×10^{-13}	1.088×10^{-4}	2.285×10^{-13}	0.9089
0.9	2.297×10^{-13}	1.206×10^{-4}	2.531×10^{-13}	0.9076
1.0	2.515×10^{-13}	1.320×10^{-4}	2.771×10^{-13}	0.9076
2.0	4.235×10^{-13}	2.235×10^{-4}	4.692×10^{-13}	0.9025
3.0	5.585×10^{-13}	2.937×10^{-4}	6.166×10^{-13}	0.9057
4.0	6.779×10^{-13}	3.543×10^{-4}	7.438×10^{-13}	0.9114
5.0	7.853×10^{-13}	4.087×10^{-4}	8.580×10^{-13}	0.9153
6.0	8.924×10^{-13}	4.615×10^{-4}	9.690×10^{-13}	0.9210
7.0	9.986×10^{-13}	5.135×10^{-4}	1.078×10^{-12}	0.9261
8.0	1.101×10^{-12}	5.629×10^{-4}	1.182×10^{-12}	0.9314
9.0	1.206×10^{-12}	6.121×10^{-4}	1.285×10^{-12}	0.9384
10.0	1.309×10^{-12}	6.626×10^{-4}	1.391×10^{-12}	0.9406

Table F2: Beta data for skin dose rate coefficients

Source Energy	Method 1 Dose Rate Coefficient (Gy Bq^{-1} s^{-1})	Method 2 Energy Deposited (MeV)	Method 2 Dose Rate Coefficient (Gy Bq^{-1} s^{-1})	Ratio
1.0	0	0	0	-
2.0	5.873×10^{-13}	8.686×10^{-4}	1.824×10^{-12}	0.3220
3.0	4.094×10^{-12}	4.413×10^{-3}	9.265×10^{-12}	0.4418
4.0	6.484×10^{-12}	6.172×10^{-3}	1.296×10^{-11}	0.5003
5.0	7.765×10^{-12}	7.255×10^{-3}	1.523×10^{-11}	0.5098
6.0	8.463×10^{-12}	7.806×10^{-3}	1.639×10^{-11}	0.5164
7.0	8.907×10^{-12}	8.120×10^{-3}	1.705×10^{-11}	0.5224
8.0	9.208×10^{-12}	8.335×10^{-3}	1.750×10^{-11}	0.5262
9.0	9.430×10^{-12}	8.472×10^{-3}	1.779×10^{-11}	0.5301
10.0	9.605×10^{-12}	8.598×10^{-3}	1.805×10^{-11}	0.5321